National Library of Canada
Acquisitions and Bibliographic Services Branch
395 Wellington Street
Ottawa, Ontario
K1A 0N4

Bibliothèque nationale du Canada
Direction des acquisitions et des services bibliographiques
395, rue Wellington
Ottawa (Ontario)
K1A 0N4

Your file Votre référence

Our file Notre référence

NOTICE

The quality of this microform is heavily dependent upon the quality of the original thesis submitted for microfilming. Every effort has been made to ensure the highest quality of reproduction possible.

If pages are missing, contact the university which granted the degree.

Some pages may have indistinct print especially if the original pages were typed with a poor typewriter ribbon or if the university sent us an inferior photocopy.

AVIS

La qualité de cette microforme dépend grandement de la qualité de la thèse soumise au microfilmage. Nous avons tout fait pour assurer une qualité supérieure de reproduction.

S'il manque des pages, veuillez communiquer avec l'université qui a conféré le grade.

La qualité d'impression de certaines pages peut laisser à désirer, surtout si les pages originales ont été dactylographiées à l'aide d'un ruban usé ou si l'université nous a fait parvenir une photocopie de qualité inférieure.

Canada

Synthesis of Microwave Structures by Inversion of the TLM Process

by

Michel Forest

A thesis presented to
The School of Graduate Studies and Research
of the University of Ottawa
in partial fulfillment of the requirements
for the degree of
Master of Applied Science in Electrical Engineering

Ottawa-Carleton Institute
for Electrical Engineering

ISBN 0-315-93616-9

Canada

UNIVERSITÉ D'OTTAWA
UNIVERSITY OF OTTAWA

Abstract

This thesis presents a novel numerical synthesis technique based on the time reversal property of the Transmission-Line Matrix method (TLM). It allows the designer to generate the geometry of a passive circuit from its desired frequency response using alternate forward and backward time-domain analyses. This approach opens new doors in microwave synthesis and offers an advantageous alternative to the traditional synthesis techniques using frequency domain analysis. To demonstrate and validate the procedure, an inductive obstacle inside a waveguide will be synthesized.

Sommaire

Cette thèse présente une nouvelle technique de synthèse numérique permettant d'effectuer la conception de structures électromagnetiques à partir de spécifications données sous forme de réponse en fréquence. Elle est fondée sur la propriété d'inversion du temps de la méthode TLM (*Transmission-Line Matrix*) et utilise en alternance des analyses directes et inversées. La conception d'une structure inductive à l'intérieur d'un guide d'onde est utilisée en guise d'exemple pour illustrer et valider les différentes étapes de la procédure. Les résultats démontrent que cette nouvelle approche temporelle offre une alternative avantageuse face aux techniques traditionelles qui utilisent plutôt des analyses fréquentielles.

Acknowledgements

I would like to express my gratitude to my supervisor Dr. Wolfgang J.R. Hoefer and my co-supervisor Dr. Michel Ney for their continuous encouragement throughout this work.

Special thanks are due to Mr. Poman P.M. So, and to all the members of the microwave group for many helpful discussions.

I would like to thank the Natural Science and Engineering Research Council of Canada for granting me a scholarship for the years 1990 to 1992.

Professors Albert Papiernik and Dominique Pompei should also be acknowledged for their interesting discussions during my stay at the Université de Nice - Sophia Antipolis.

Very special thanks are due to Jean-François Huard for proofreading this thesis.

I would also like to thank the students of the microwave group of the University of Ottawa and especially Sylvain, Redouane and Myke for many comments on my work.

Finally, I would like to express my sincere appreciation to my wife Caroline, for supporting me during my work and specially during the writing of this thesis.

À Caroline

Contents

List of Figures

List of Tables

Chapter 1

Introduction

1.1 Overview

The need for more efficient design tools has always been obvious. The epoch when the designer had to build a few costly prototypes before providing a good product is long past. Today, computer simulations are an important part in the design process. With efficient simulation techniques, it is now possible to produce better results faster at a lower price because computers are able to perform the task faster and with greater flexibility. Overall, with the advent of cheap memory and fast processors, it is possible to simulate very large structures in a fairly small amount of time. These

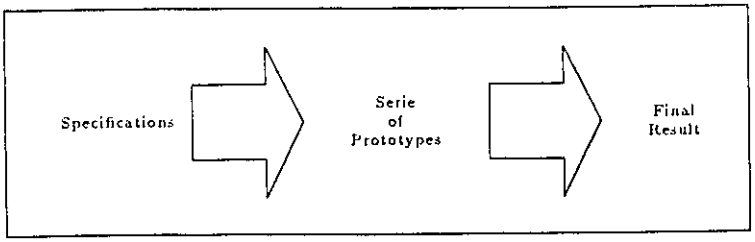

Figure 1.1: Design process before the advent of digital computers.

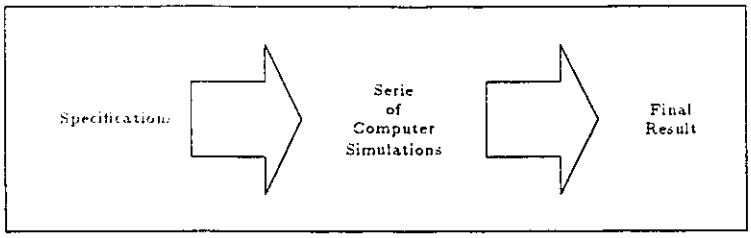

Figure 1.2: Design process using computer simulations

days, computers are becoming powerful enough to suggest that they could not only perform simulations but also design of simple products by themselves. Provided with appropriate specifications, computers are able to find the optimum values of some parameters the device to be designed. Many techniques can be used to achieve such a goal. Most of them are based on a frequency domain analysis technique combined with an optimization strategy. These techniques are currently applied in many fields, such as the design of thermal structures in mechanical engineering, the design of digital circuits or electromagnetic structures in electrical engineering, or fluid mechanics in civil engineering. However, time-domain numerical techniques are not well suited for this kind of design approach since every analysis requires the transient buildup of the time response from an impulsive excitation which involves a large computation time. Thus, the repeated analyses would be very wasteful. Hence, a different approach should be taken to perform the synthesis in the time-domain.

This thesis reports a novel technique for the synthesis of conducting scatterers based on alternate forward and backward analyses without requiring traditional optimization procedures. It takes advantage of the time dimension since each time-domain analysis provides full frequency band information. It is the result of a study to use time reversal of the TLM method to perform the synthesis of electromagnetic structures, conducted by Sorrentino et al. [1] in 1991. Results show that it offers an

interesting alternative to the traditional synthesis techniques which have been used so far.

1.2 Original Contributions of this Thesis

The following original contributions were made while investigating the time reversal property of the Transmission-Line Matrix method.

- The development of an accurate technique for reconstructing the image of a metallic scatterer from its TLM time response. Based on the principles introduced in [1], several techniques for precise description of a metalic obstacle, using the field components available from a TLM analysis, were developed.
- The development of a new synthesis procedure based on the shape reconstruction technique using time reversal. This procedure includes a novel technique for modifying the responses of TLM analyses.
- The implementation of the new synthesis procedures on a massively parallel computer, the Connection Machine.

So far, no previous work using a numerical time reversal procedure has been published. The synthesis technique presented here is completely new in the field of numerical modeling as applied to the design of microwave structures.

1.3 Thesis Outline

After this introduction, Chapter 2 gives a short overview of the Transmission-Line Method. In Chapter 3, the technique of shape reconstruction is presented, and a programming technique will be demonstrated. Its purpose is to clearly demonstrate how to reconstruct the shape of a previously analysed obstacle by reversing the TLM

process. Chapter 4 then presents the complete synthesis procedure which is based on the shape reconstruction technique. Numerical results are presented in Chapter 5, and the parallelization of the technique is explained in Chapter 6. Finally, the Conclusion summarizes the thesis and presents several applications of this novel procedure in some other areas.

Chapter 2

The Transmission-Line Matrix Method

The Transmission-Line Matrix (TLM) method was first introduced by Johns and Beurle [2] in the early seventies. It is a discrete time and discrete space sampling method for modeling the propagation of electromagnetic waves. The propagation space is represented by a mesh of interconnected transmission lines. This chapter presents the different aspects of this numerical technique. For the purpose of this project, the two-dimensional version of the method will be emphasized. Application to 3D problems is only presented as an improvement of the research project in Section 3.5.

2.1 Propagation of Electromagnetic Waves

The TLM method is a discretized version of Huygens' principle. The latter specifies that each wave front created by a radiating source can be represented by a new series of sources, which in turn, create a new series of wave fronts. To model the wave propagation space, the TLM method employs a grid of interconnected transmission

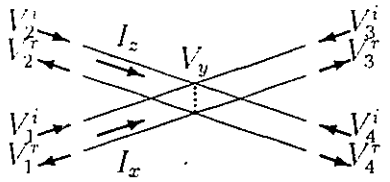

Figure 2.1: Two-dimensional TLM shunt node.

lines with specific line parameters. The propagation of electromagnetic waves is represented, in the TLM mesh, by the movement of voltage impulses along the transmission lines. The differential equations which rule the voltages and the currents on the lines are of the same form as Maxwell's equations. Therefore, a relation can be established between the electromagnetic fields in the medium and the voltages and currents in the TLM mesh. The differential equations relating the currents and the voltage for the well known two-dimensional shunt node shown in Figure 1.1 are:

$$\frac{\partial V_y}{\partial x} = -L\frac{\partial I_x}{\partial t}, \tag{2.1}$$

$$\frac{\partial V_y}{\partial z} = L\frac{\partial I_z}{\partial t}, \tag{2.2}$$

$$\frac{\partial I_z}{\partial z} + \frac{\partial I_x}{\partial x} = -2C\frac{\partial V_y}{\partial t}, \tag{2.3}$$

where L and C are the inductance and the capacitance per unith length of the elementary transmission line, while V_y, I_x and I_z are the voltage at the TLM node and the currents in the mesh. Setting $\frac{\partial}{\partial y} = 0$, the following equations are derived from the Maxwell's equation:

$$\frac{\partial E_y}{\partial x} = -\mu\frac{\partial H_z}{\partial t}, \tag{2.4}$$

$$\frac{\partial E_y}{\partial z} = \mu\frac{\partial H_x}{\partial t}, \tag{2.5}$$

$$\frac{\partial H_x}{\partial z} + \frac{\partial H_z}{\partial x} = \epsilon\frac{\partial E_y}{\partial t} \tag{2.6}$$

where E_y, H_x and H_z are the orthogonal electric and magnetic field components in the x, y and z directions. Equations (1.1) to (1.3) can be combined to obtain a two-dimensional wave equation for the voltages in the network as a function of time and space

$$\frac{\partial^2 V_y}{\partial x^2} + \frac{\partial^2 V_y}{\partial z^2} = 2LC\frac{\partial^2 V_y}{\partial t^2} = \frac{1}{v_n^2}\frac{\partial^2 V_y}{\partial t^2}. \tag{2.7}$$

In the same manner we obtain for the electric field

$$\frac{\partial^2 E_y}{\partial x^2} + \frac{\partial^2 E_y}{\partial z^2} = \mu\epsilon\frac{\partial^2 E_y}{\partial t^2} = \frac{1}{v_n^2}\frac{\partial^2 E_y}{\partial t^2} \tag{2.8}$$

where v_n is the velocity of the wave in the medium. This yields the following correspondence between the field components in the medium, and the voltage and currents in the TLM mesh :

$$E_y = V_y, \tag{2.9}$$

$$H_x = -I_z, \tag{2.10}$$

$$H_z = I_x, \tag{2.11}$$

with the constitutive parameters ϵ and μ related to line parameters L and C as

$$\epsilon = 2C, \tag{2.12}$$

$$\mu = L. \tag{2.13}$$

The velocity of the wave described by equation 1.7 is then given by

$$v_n = \frac{1}{\sqrt{2LC}}. \tag{2.14}$$

However, for the elementary transmission line of parameters L and C, the wave velocity is

$$v_l = \frac{1}{\sqrt{LC}}, \tag{2.15}$$

which is equal to the speed of light c in the case of air filled transmission lines. Therefore the velocity in the TLM mesh is $1/\sqrt{2}$ times the velocity on the elementary transmission lines.

In a two-dimensional homogeneous medium, the currents and the voltage at each node in the mesh can be evaluated as

$$V_y = \frac{1}{2}[V_1^i + V_2^i + V_3^i + V_4^i], \tag{2.16}$$

$$I_x = \frac{V_4^i - V_2^i}{Z_o}, \tag{2.17}$$

$$I_z = \frac{V_1^i - V_3^i}{Z_o}, \tag{2.18}$$

where the V_j^i represent the voltage impulses incident on each node and Z_o is the intrinsic impedance of the medium. Thus, by selecting the proper values of line parameters (L and C), the TLM mesh will model a realistic medium of propagation.

At each point in the mesh, the impulses are scattered so as to respect the conservation of energy. The scattering of incident voltage impulses at every time step k yields the reflected impulses at each node. For the homogeneous medium we have:

$$\begin{bmatrix} V_1 \\ V_2 \\ V_3 \\ V_4 \end{bmatrix}_{k+1}^{r} = \frac{1}{2} \begin{bmatrix} -1 & 1 & 1 & 1 \\ 1 & -1 & 1 & 1 \\ 1 & 1 & -1 & 1 \\ 1 & 1 & 1 & -1 \end{bmatrix} \begin{bmatrix} V_1 \\ V_2 \\ V_3 \\ V_4 \end{bmatrix}_{k}^{i} \tag{2.19}$$

Once reflected from the nodes, the impulses are incident on the neighbouring nodes and the scattering continues with the new set of incident impulses.

$$V_k^r \Longrightarrow V_{k+1}^i \tag{2.20}$$

The scattering and exchange of impulses between the nodes in the mesh are the basis of the TLM algorithm as shown in Figure 1.2. Since the travel time between equally spaced nodes is constant, we say that the process is synchronous. Let denote the

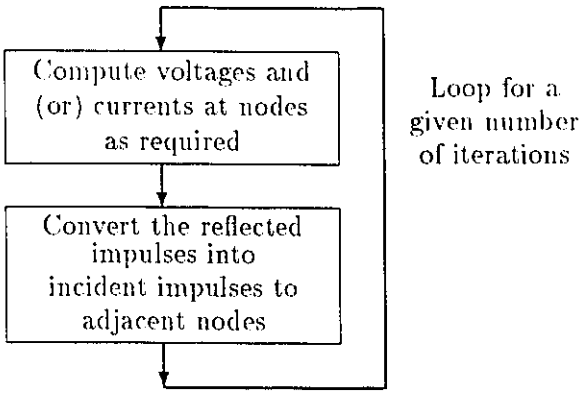

Figure 2.2: Basic algorithm of the TLM method

distance between nodes as Δl. We also set the computational time step equal to Δt. The two parameters are related by the wave velocity v_l in the elementary transmission lines

$$\Delta t = \frac{\Delta l}{v_l}. \tag{2.21}$$

Figure 1.3 illustrates how a single impulse incident on a node can propagate through the mesh at every time step (for the two-dimensional case). Due to the discretization of the medium, some errors are introduced in the velocity of the wave propagating in the mesh. These errors and their corrections are well described in [3, 4, 5].

Finally, the scattering matrix equation corresponding to the more general case where the shunt nodes are loaded with permitivity and loss stubs is:

$$\begin{bmatrix} V_1 \\ V_2 \\ V_3 \\ V_4 \\ V_5 \end{bmatrix}^r_{k+1} = \frac{1}{y} \begin{bmatrix} -(y-2) & 2 & 2 & 2 & 2y_o \\ 2 & -(y-2) & 2 & 2 & 2y_o \\ 2 & 2 & -(y-2) & 2 & 2y_o \\ 2 & 2 & 2 & -(y-2) & 2y_o \\ 2 & 2 & 2 & 2 & (2y_o - y) \end{bmatrix} \begin{bmatrix} V_1 \\ V_2 \\ V_3 \\ V_4 \\ V_5 \end{bmatrix}^i_k \tag{2.22}$$

with

$$y = 4 + y_o + g_o \tag{2.23}$$

where y_o and g_o are the normalized characteristic admittances of the permitivity stub and loss stub respectively, as illustrated in [2].

2.2 Limitation of the Computational Domain

Even if large computer memory is available, the extent of the structure modeled by the TLM mesh must be limited. Boundaries are used to restrict the computational domain. Except for closed structures, absorbing boundary conditions are used to

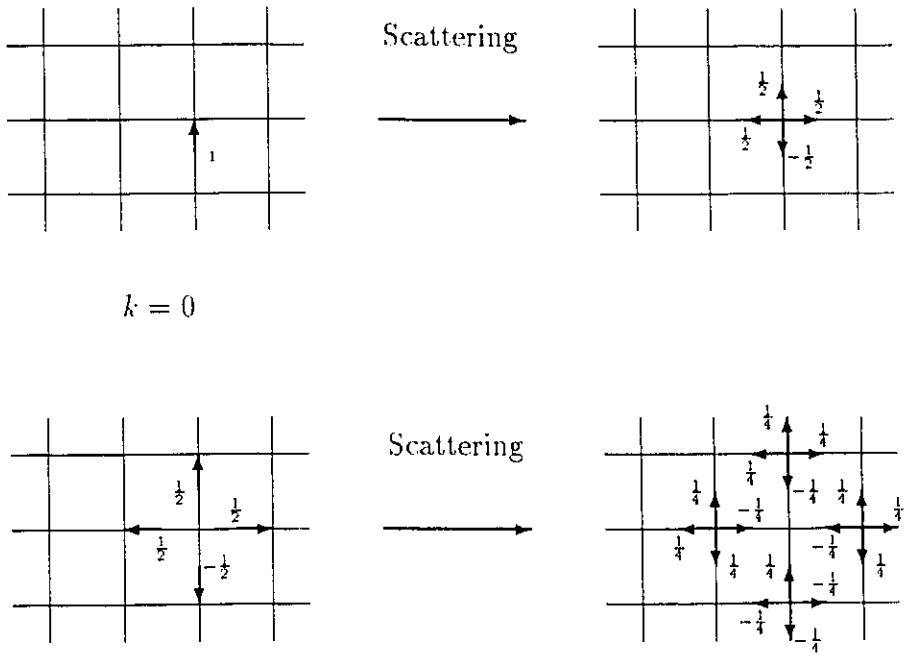

Figure 2.3: Example of the propagation process in a two-dimensional mesh after the injection of an impulse.

model the propagation of the electromagnetic waves out of the structure. For example, to simulate a discontinuity in a long waveguide, absorbing boundaries are used to restrict the computational domain to a small region around the discontinuity. The equivalence between fields and voltages or currents in the mesh suggests that this could be achieved by using a proper reflection coefficient ρ while depends on the desired type of boundary. In the shunt connected two-dimensional TLM node, ideal electric and magnetic walls are represented by a -1 and $+1$ reflection coefficient, respectively. They are inserted half-way between the nodes to preserve the synchronism with other impulses in the network. An absorbing boundary can be simulated by adjusting the coefficient ρ to the reflection on a general boundary of surface impedance Z_c.

$$\rho = \frac{Z_c - Z_o}{Z_c + Z_o} \tag{2.24}$$

However this model is valid only for a narrow frequency band if Z_c is dispersive.

Other techniques for modeling absorbing boundaries over a wide frequency band have been developped [6] or are under study. Among others, the Johns matrix technique which is based on time-domain diakoptics, provides good absorption over a large frequency band. Figure 1.4 illustrates how boundaries are included in a TLM mesh. Note the distance of $\Delta l/2$ between the nodes and the boundaries.

2.3 Excitation and Response

While the TLM method is a time-domain numerical technique, typical applications require results in the frequency domain. A single impulse excitation of the TLM mesh provides a full bandwidth response in only one analysis. Mathematically, the impulses propagating through the TLM mesh are functions which take a finite value at the time k and are zero elsewhere. Thus, they do not correspond exactly to the Dirac distribution δ. Let $f(t)$ denote the response obtained from a TLM analysis at

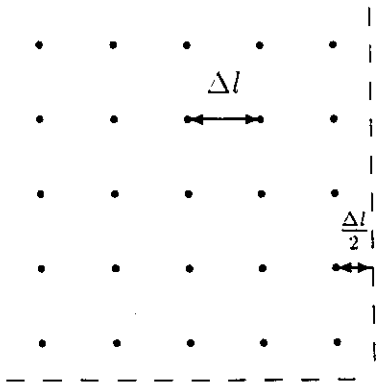

Figure 2.4: Insertion of a wall into a 2D-TLM mesh

a specific node. Equation (1.25) illustrates the results of the time-domain analysis of a structure. At a selected output node, the value of the node voltage V_y is taken at each time step k. The discrete Fourier transform (DFT) of $f(t)$ is then taken.

$$f(t) = \sum_{k=0}^{\infty} V_y \delta(t_0 - k\Delta t) \tag{2.25}$$

$$F(\omega) = \mathcal{F}(f(t)) \tag{2.26}$$

For a single frequency excitation, one has the possibility to use a series of impulses which sample a sine wave; a Gaussian envelope can be selected for a pulse for a band-limited excitation. It is interesting to mention that the excitation of the structure can be done at any node in the mesh.

2.3.1 Evaluation of the Scattering Parameters

Scattering parameters –or S parameters– are used to provide transmission and reflection characteristics of structures under study. A procedure has been developed to

extract those parameters from a TLM analysis [7].

Usually, the structure under study is symetrical and only two parameters need to be evaluated: the reflection and the transmission coefficients S_{11} and S_{21}. Thus, provided the incident, reflected and the transmitted voltages are known, one can compute the value of both S_{11} and S_{21}. They are evaluated according to the following expressions:

$$S_{11} = \frac{V_{out1} - V_{out0}}{V_{out0}} \tag{2.27}$$

$$S_{21} = \frac{V_{out2}}{V_{out0}} \tag{2.28}$$

where V_{out0} is the reference or incident voltage obtained from a simultaneous analysis of an empty matched waveguide section of identical cross-section, V_{out1} is the voltage mesured at the input of the filter (containing both the incident and the reflected waves) and V_{out2} is the voltage taken at the output of the same filter (containing the transmitted wave). All those responses are in the frequency domain. A Fourier transform is used to get them from the time-domain responses obtained by TLM analysis.

To explain this procedure, let us look at the following example: suppose that we want to extract the S parameters of a waveguide filter which contains two circular posts. Its topology is shown in Figure 1.5. The excitation consists of a set of impulses with half-sine distribution to launch the dominant TE_{10} mode. There are two nodes where the field response will be picked-up, at the input and at the output. The first one will provide the information on the combined incident and the reflected voltages while the second one will give the transmitted voltage. To extract the reflected voltages from the total voltage mesured at the input, a short section of the same waveguide without the obstacles is used with the same excitation. The value V_{out0} picked-up in this empty structure provides the incident voltage since no reflection occurs in this waveguide.

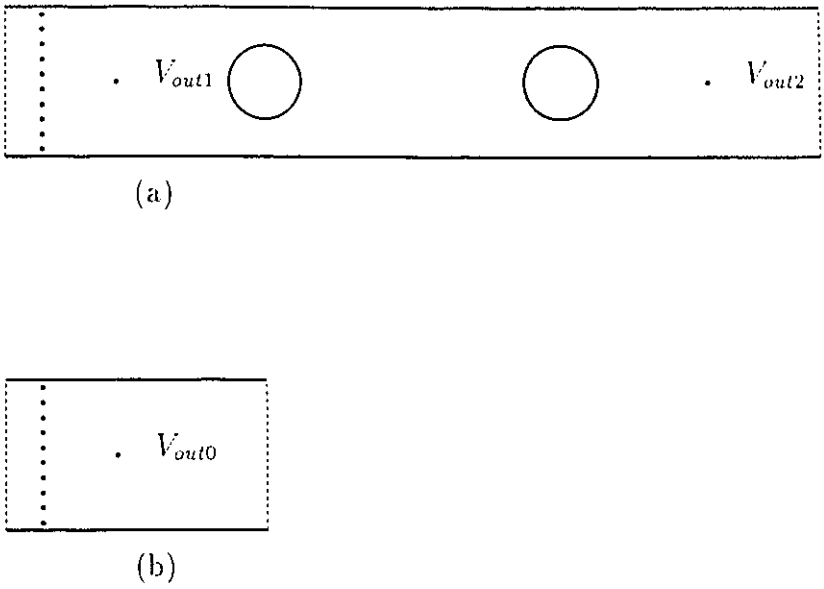

Figure 2.5: (a) Rectangular waveguide filter with output points for S parameters extraction. (b) Short section of the same waveguide for the reference signal.

After Fourier transform of those time domain signals, the frequency domain solutions are obtained. Using equations (1.27) and (1.28), the scattering parameters are calculated.

Experience has shown that the output points must be far enough from the discontinuities to get only the dominant mode response. This constrains us to extend the computational domain, thus increasing the computational time as well. To improve this situation, one can use a Fourier series expansion over the transversal dimension of the guide at every time step near the discontinuities, thus reducing the size of the mesh. It will result in a separation of the amplitudes of every modes. By extracting the Fourier serie coefficient corresponding to the mode, of interest, at every time step, it is possible to build a time-domain signal for a single mode of propagation. Usually, the mode of interest is the dominant mode. For more details about this technique, refer to Section 4.3 which deals with the extraction of the dominant mode response of a structure.

2.4 The Time Reversal of the TLM Method

The TLM method, as well as the other time-domain numerical techniques are relatively new in the field of numerical modeling of electromagnetic structures. So far, their use is limited to the conventional time-domain analysis of structures. Other avenues still remain to be investigated. In this section, an important property of the TLM method, the time reversal property, is presented. This property provides new ways of designing microwave structures. In particular, it is the idea behind the new TLM synthesis technique presented in this thesis.

2.4.1 Inversion of the Algorithm

The TLM algorithm consists of a series of scattering iterations performed at each node. Recall that the basic matrix equation for the two-dimensional TLM scattering is

$$\begin{bmatrix} V_1 \\ V_2 \\ V_3 \\ V_4 \\ V_5 \end{bmatrix}^r_{k+1} = \frac{1}{y} \begin{bmatrix} -(y-2) & 2 & 2 & 2 & 2y_o \\ 2 & -(y-2) & 2 & 2 & 2y_o \\ 2 & 2 & -(y-2) & 2 & 2y_o \\ 2 & 2 & 2 & -(y-2) & 2y_o \\ 2 & 2 & 2 & 2 & (2y_o - y) \end{bmatrix} \begin{bmatrix} V_1 \\ V_2 \\ V_3 \\ V_4 \\ V_5 \end{bmatrix}^i_k \tag{2.29}$$

where y and y_o are variables related to the dielectric constant and loss parameter. In this system of equations, the impulses incident on each nodes are used to compute the reflected impulses. This is done iteratively each time step at every node.

Also, it is easy to verify that the scattering matrix is equal to its inverse.

$$S = S^{-1} \tag{2.30}$$

This means that it is possible to obtain the values of the incident impulses from the knowledge of the reflected impulses without any modification of the algorithm since the basic matrix equation remains the same. This results in a time reversal of the TLM method. Instead of using the TLM method to obtain the field distribution in time and space from a given source, it could be used backwards to obtain the excitation corresponding to a given field distribution.

This property was first illustrated by Sorrentino, So and Hoefer [1] and was presented for the first time at the European Microwave Conference in 1991.

2.4.2 Applications

An important advantage of time-domain simulations is the possibility to visualize the actual propagation of waves in any structure. This makes the TLM method an interesting tool in educational electromagnetics. Time-domain simulations help the understanding of dynamic phenomena described by Maxwell's equations using visual animation. With the time reversal of the TLM method, it is now possible to stop a forward simulation at any given time step and proceed with the backward simulation. This helps in visualizing a specific effect during a simulation by alternating between forward and backward time steping.

Although the educational aspect of this feature is important, the main application of this new property of the TLM method lies in the ability to obtain a source from the field distribution it creates. The TLM method can be used to reconstruct the source from a field distribution by reversing the time sequence. As an example, Figure 1.6 shows a series of images describing this process.

In the example a structure surrounded by metalic walls is analysed, and the process is reversed after several iterations. In (a), the structure is displayed with the initial excitation which consist of a single impulse at a node in the structure. Figure 1.6 (b) and (c) show the structure after 20 and 100 iterations. After 200 iterations, the process has been stopped and started in the reverse time sequence to finally obtain the reconstructed source in (d). This reconstructed source is identical to the original one. This example shows the simplicity of reconstructing a source using the time reversibility property of the TLM method.

2.5 Conclusion

This chapter has presented the Transmission-Line Matrix method which is a technique based on Huygens' principle to simulate the propagation of electromagnetic waves.

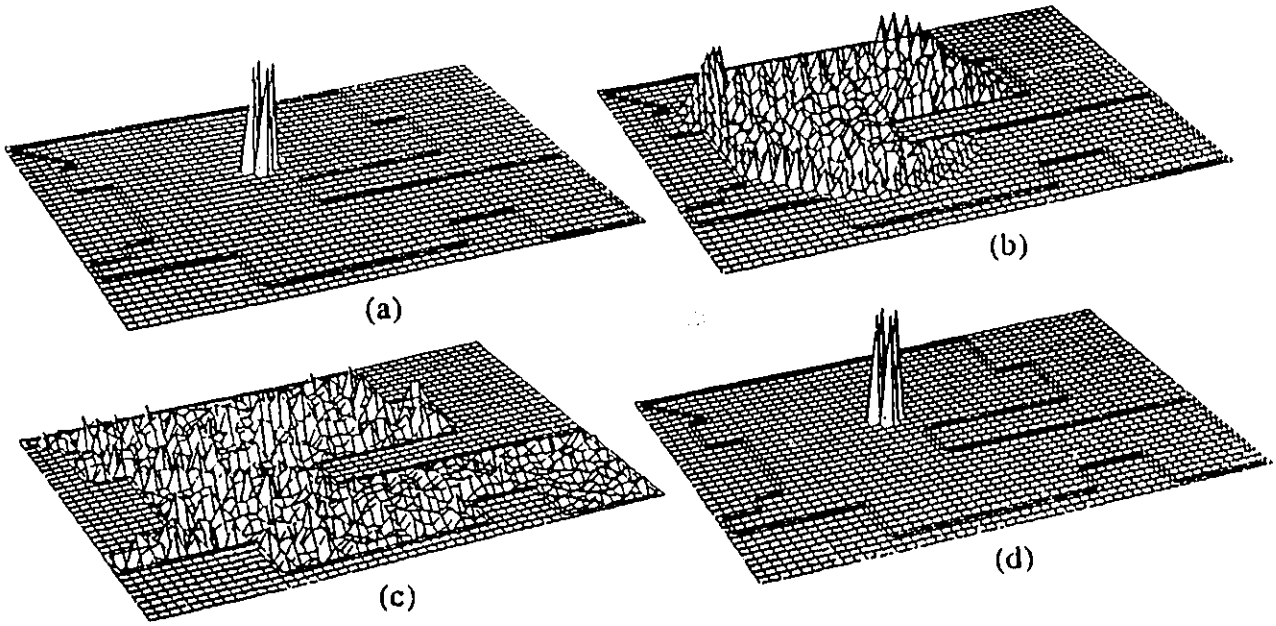

Figure 2.6: Example demonstrating the time reversibility of the TLM method. In (a) (b) and (c), the field set up by an impulse in the structure under study is displayed at $t = 1$, $t = 20$ and $t = 100$ respectively. After the inversion of the time sequence, the source has been reconstructed as displayed in (d).

The application of this time-domain numerical technique to the analysis of general structures was shown. Finally, the property of time reversal of the TLM method reveals promissing avenues in the field of time-domain synthesis of structures.

Chapter 3

The Technique of Shape Reconstruction

The time reversal property of the TLM method can be used to develop a new technique of shape reconstruction. This chapter shows how the TLM method can be used to reconstruct the shape of a metallic scatterer that has previously been analysed. The procedure is explained in detail, and some examples of reconstruction are presented.

3.1 Scattering of an Incident Wave by a Metallic Obstacle

When a wavefront is incident upon a metallic obstacle, a perturbation of the field quantities is created due to the surface currents induced on the obstacle. The tangential electric field $\vec{E}$ is related to the surface current density $\vec{J}$ by the following expression:

$$\vec{J} = \sigma \vec{E}, \tag{3.1}$$

where σ is the conductivity of the obstacle.

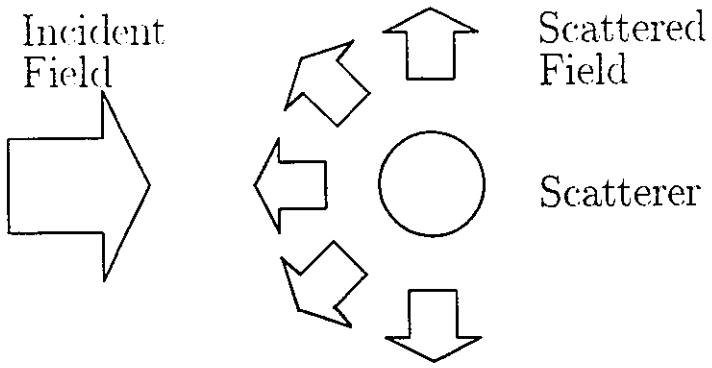

Figure 3.1: Incident and scattered field around a metallic obstacle.

After the wavefront has hit the obstacle, it becomes difficult to separate the incident and the scattered electromagnetic fields. However, it is possible to separate these two fields if we know the current distribution on the surface of the obstacle and the value of the incident electromagnetic field. This can be achieved easily using numerical techniques such as the method of moments. This method builds a system of equations using the Green's function approach which is then solved for the current distribution. Using Maxwell's equations, the scattered field due to this current distribution on the obstacle can be obtained.

The possibility to separate the incident and the scattered field quantities suggests that by applying the time reversal property to the scattered electromagnetic field, it would be possible to obtain the induced sources in the same way as we can find the initial sources from a known electromagnetic field distribution (see Chapter 2). This idea leads to the technique of shape reconstruction.

Because of the linearity of the TLM method, the principle of superposition can be applied. Therefore, the impulse response due to two different sources is equal to the sum of the impulse reponses to each source, taken separately. Let the TLM time-domain reponse at an output node O be denoted by $\phi(t)$. Let us also assign $\phi_1(t)$ and $\phi_2(t)$ to the responses to two different excitations. Thus, the total response

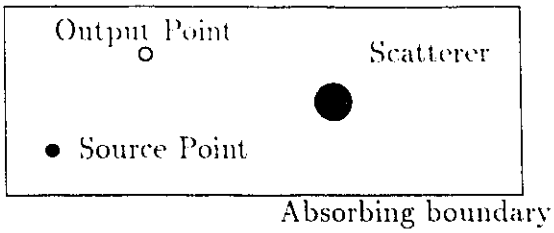

Figure 3.2: The entire structure including the scatterer yielding the total solution

to the combined excitations is

$$\phi_T(t) = \phi_1(t) + \phi_2(t). \tag{3.2}$$

This illustrates how the principle of superposition can be applied to the TLM method. Naturaly, it can also be used to separate the incident and scattered field responses. In other words, one can separate the effects of the primary and the induced sources in a linear TLM simulation. In the present case, we want to extract the field response to the induced sources from the combined response due to both primary and induced sources.

Let us now introduce a new notation to facilitate the understanding of the problem. If $\phi_T(t)$ denotes the total field solution, $\phi_H(t)$ the homogeneous solution (incident field without the scatterer), then according to the principle of superposition, we can write the particular solution as

$$\phi_P(t) = \phi_T(t) - \phi_H(t), \tag{3.3}$$

where $\phi_P(t)$ represents the field solution corresponding to the induced sources on the contour of the obstacle.

Consequently, the total response can be obtained at any node of the TLM model simply by analyzing the scattering problem. To obtain the homogeneous solution, the scatterer is removed, while all the other features of the problem remain the same. The difference between the total and the homogeneous field solutions yields the particular solution. The objective of this separation of the responses is to use the particular

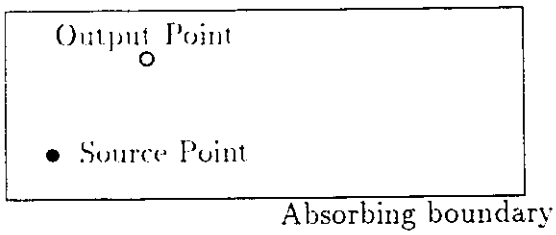

Figure 3.3: Empty structure yielding the homogeneous solution.

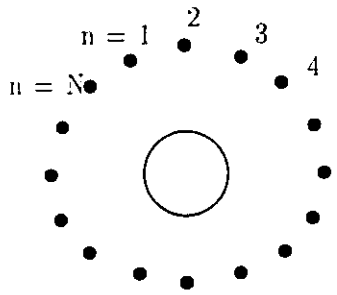

Figure 3.4: Structure using a surrounding sources.

solution in a backward simulation to provide information about the induced sources. However, using a single node as output point does not provide enough information to accurately reconstruct the induced sources.

In order to fully describe the location of the induced sources by reversing the TLM method, information about the distribution of the fields in space is essential. For example, if we surround an obstacle by N nodes numbered from 1 to N, as seen in Figure 3.4, and use them as output points for the analysis, and as input points for the injection of the inverse sequence, the reconstruction would be more efficient.

The total and the homogeneous field solutions $\phi_T(n,t)$ and $\phi_H(n,t)$ are functions of space and time. The inverse simulation yields the induced sources. These induced sources indicate the contour of the metallic obstacle. Therefore, a reconstruction of the shape of the obstacle is possible.

In the example of the reconstruction of an impulsive source (Figure 1.6) by revers-

ing the time sequence after an analysis, the inverse process led to a single source at time $t = 0$. When analysing a structure containing a metallic scatterer, the sources on the contour of this obstacle are not induced simultaneously. In fact, the wavefront that hits the obstacle creates a series of asynchronous induced sources. Therefore, when using the inverse process to obtain these induced sources, parts of the contour will appear at different time steps. For that reason, the reverse process is not able to reconstruct all the induced sources simultaneously. Many solutions have been suggested to overcome this problem.

The next section presents a technique of shape reconstruction which is capable of determining the topology of the scatterer.

3.2 Presentation of the Procedure

To explain the procedure, a simple structure is used so as to not obscure the essence of the technique. Let the structure be a parallel plate waveguide contaning a metallic obstacle. This structure has been chosen because it can be treated as a two-dimensional problem since there is no physical variation in the vertical dimension. Also, such a structure can propagate a TEM mode which considerably simplifies the TLM analysis. A top view of this waveguide is represented in Figure 3.5. It is composed of two magnetic walls and two absorbing boundaries to limit the computational domain. Those absorbing walls are TEM absorbing boundaries represented by a single impulse reflection coefficient.

The analysis is performed by placing a linear set of impulsive sources on the left side of the waveguide. The dominant TEM mode is generated by injecting, at every node in the excitation zone, an impulse having the same amplitude. The wavefront then propagates through the guide toward the right until it hits the obstacle. At this moment, a reflected wave is created. During the whole process, the time-domain

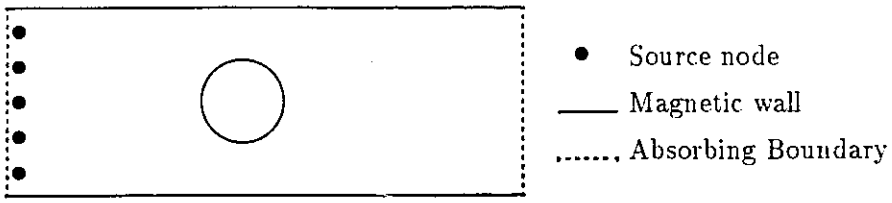

Figure 3.5: Top view of the parallel plate waveguide containing the metallic scatterer.

response can be taken at any point in the mesh. The proposed shape reconstruction procedure consists of the following three steps:

1. The complete structure including the obstacle is analysed. At every iteration, the values of the impulses incident at all nodes adjacent to the two absorbing boundaries are saved. This yields the total solution $\phi_T(n,t)$.

2. The same structure is analysed without the obstacle. Like in the first part, the impulses at both absorbing boundaries are saved to yield the homogeneous solution $\phi_H(n,t)$.

3. The difference between the total and the homogeneous solutions, which is the particular solution, is re-injected into the empty waveguide in reverse time sequence. After the entire inverse process, the induced sources on the circumference of the obstacle are obtained.

As we know, the fields propagating in the structure can be visualized in the time-domain using a mapping of the field quantities into a color scale or a 3D mesh. Since the scattered field has a local maximum or minimum at the surface of the scatterer, the value of the field at every node is updated if the current value is higher than any previous value. At the end of the process, a distribution map of the maximum field value is obtained. It is from this map that the shape of the scatterer can be extracted. Depending on the field component, a different image is obtained and

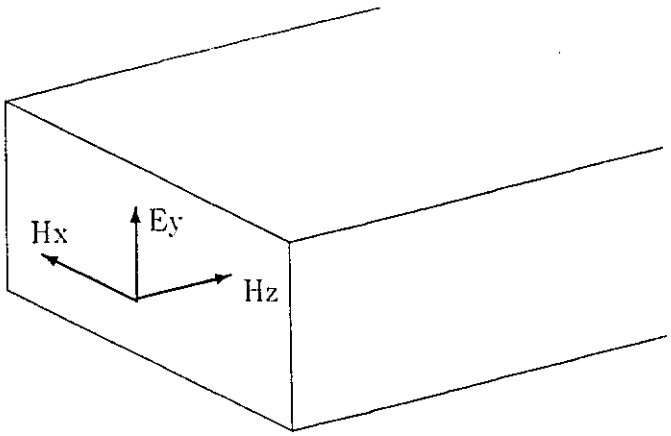

Figure 3.6: Field components used in the two-dimensional TLM analysis of a waveguide problem.

different information can be displayed. The sources used in both analyses, the first and the second parts, must be the same, and the number of iterations must be equal.

3.3 Processing of the Final Image

In the two-dimensional TLM analysis, a maximum of 3 field components can be used. In the case of a longitudinal section of a rectangular waveguide, the components needed to describe the propagation of all TE_{n0} modes are E_y, H_x and H_z. As described in chapter 2, these field components are represented by voltages and currents in the TLM mesh.

From the inverse simulation, it is possible to obtain maps of the maximum value of these field components or a combination of them. Next we show the kind of results that can be expect from these maps and how to combine them to enhance the precision of the shape reconstruction.

3.3.1 The Transverse Electric Field: E_y

By displaying the map of the maximum absolute value of the electric field during the inverse time sequence, one can get the shape and the position of the previously analysed obstacle from the location of the maximum values of the field component. If the re-injected signal of the backward simulation, which is the particular solution, is due to the induced sources, then the highest values of the electric field should correspond to the most important induced sources on the contour of the obstacle; obviously they will indicate the shape and the location of the obstacle. Figure 3.7 shows as an example, a metallic septum inside a parallel plate waveguide. The value of the field on each node in the guide is discretized and assigned an integer value between 0 and 255. The set of integer values has been chosen in order to use a color map of 256 colors or 8 bits per pixel. In this way, the shape of the obstacle is quite well described. In Figure 3.7, a contour representation is used.

To extract the dimension of an obstacle with better precision, an algorithm is used to locate of the local maximum for every line of the mesh. A criterion is used to determine at what level a maximum value is stored; this will be part of the contour. For the electric field representation, a point is considered a local maximum only if the absolute value of the slope on each side of the node in question is higher than a given level. This level has been evaluated experimentally to $Th = 6/\Delta l$. Using this threshold value with the following algorithm, the local maxima are found.

Algorithm for the extraction of the local maxima

- For each line in the structure
  - For every nodes on the line

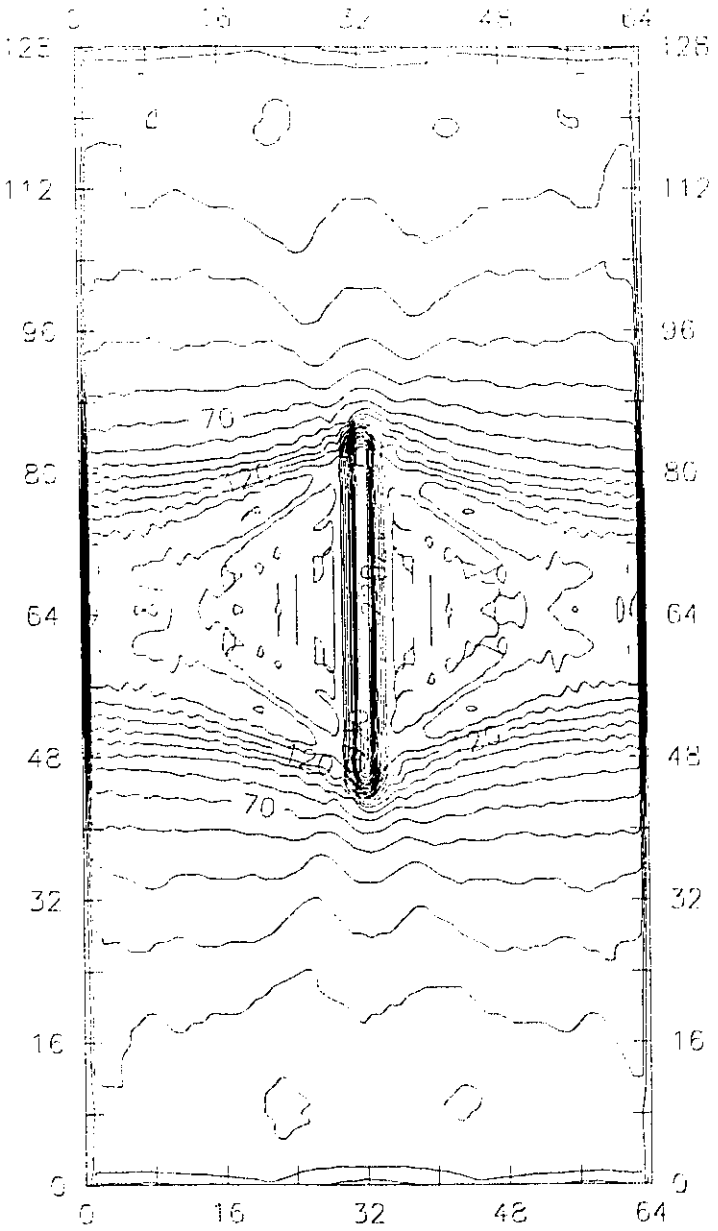

Figure 3.7: Distribution of the maximum values of the electric field obtained from a reverse TLM analysis.

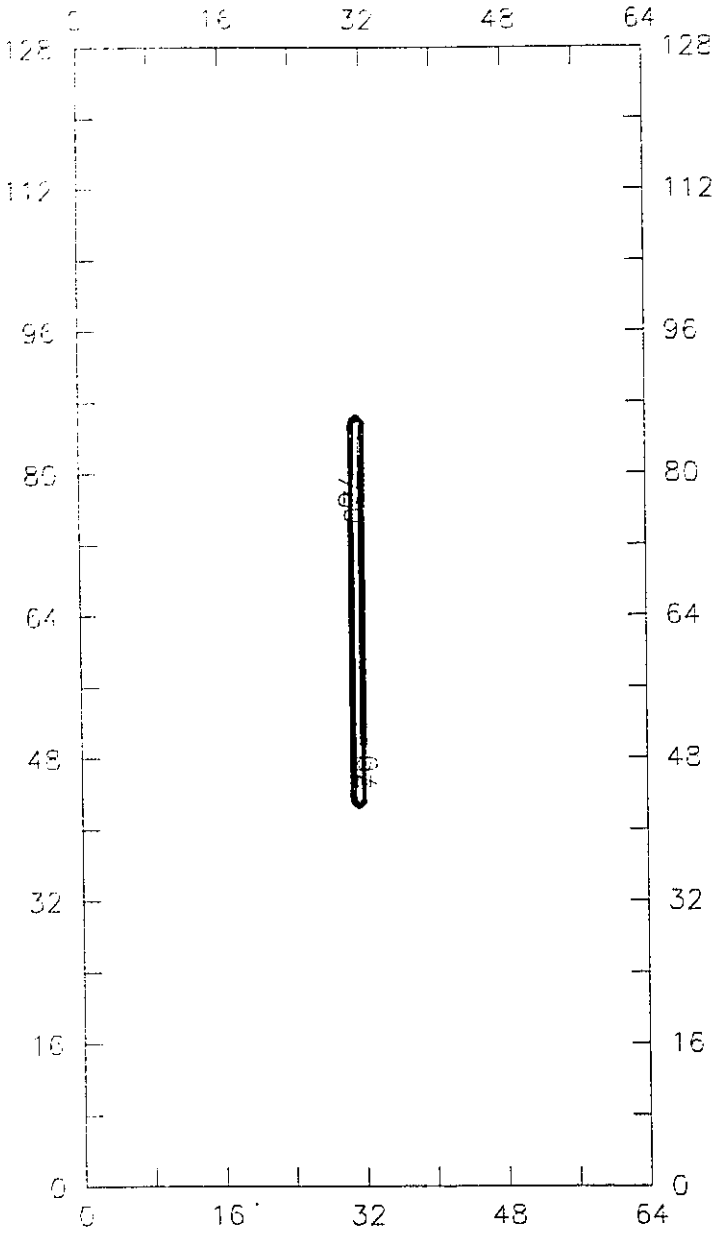

Figure 3.8: Result of the extraction of the local maxima for each line.

* If the slope on the left is larger than Th AND the slope on the right is smaller than $-Th$. Then the node is detected as a local maximum and is assigned a value "active".

The result is a map of boolean values where each active node corresponds to a detected local maximum. This map gives a good representation of the topology of the scatterer. Using this algorithm, the exact shape of the septum of Figure 3.7 has been obtained; it is displayed in Figure 3.8.

3.3.2 Transversal Magnetic Field: H_x

The transversal magnetic field component can also be used to extract the topology of an obstacle. This field component behaves in a similar way as does the electric field except that now the positions of the local minima describe the shape of the obstacle. Thus, the same processing can be done on this image except that the algorithm extracts the position of the local minima instead of the local maxima. For the example of Figure 3.7, it can be seen from Figure 3.9 that the result of the extraction of the local minima yields the same shape of septum than Figure 3.8.

3.3.3 Longitudinal Magnetic Field: H_z

The longitudinal magnetic field component does not appear when a pure TEM wave propagates. However, it is generated in the form of the higher order modes when the wave hits an obstacle, and especially at the location of the sharp edges. It might also be generated by the coarseness effet of the TLM mesh around those corners or sharp edges. When re-injecting the particular solution into the empty waveguide, this field component will mainly show the position of the corners of the obstacle. Figure 3.10 shows an example of the final longitudinal field image obtained from the inverse TLM simulation of the metallic septum.

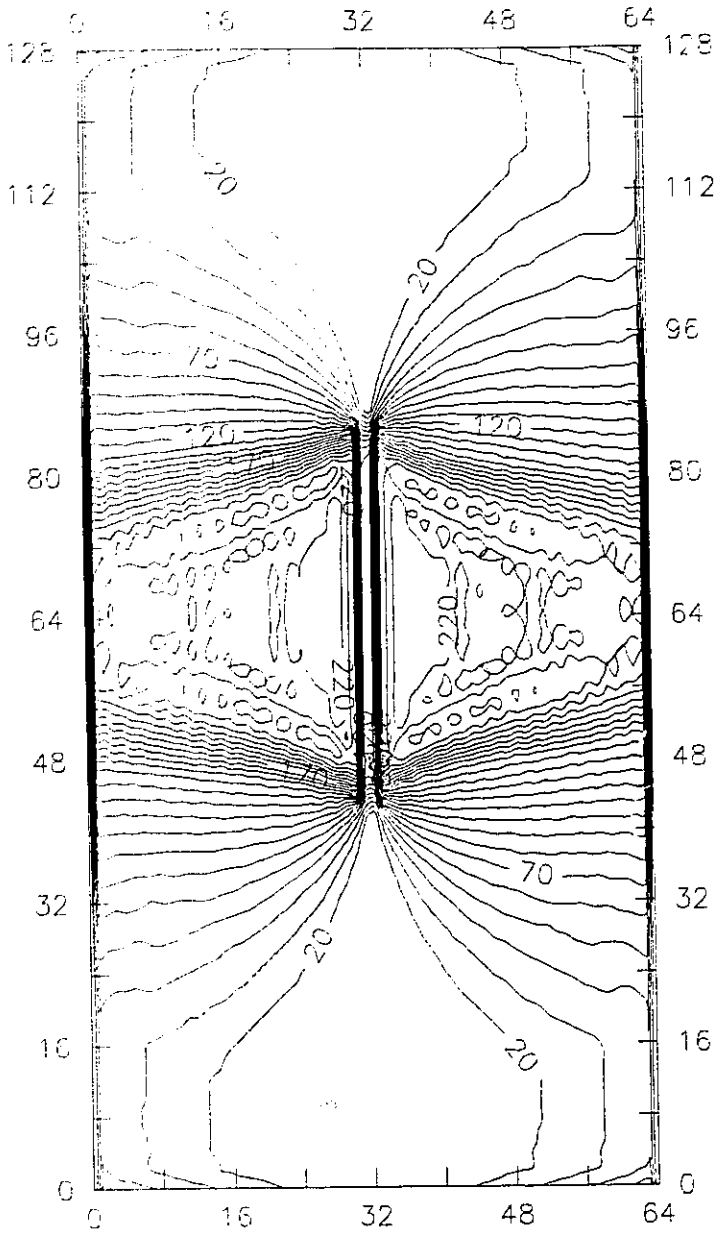

Figure 3.9: Distribution of the maximum value of the transversal magnetic field obtained from a reverse TLM analysis.

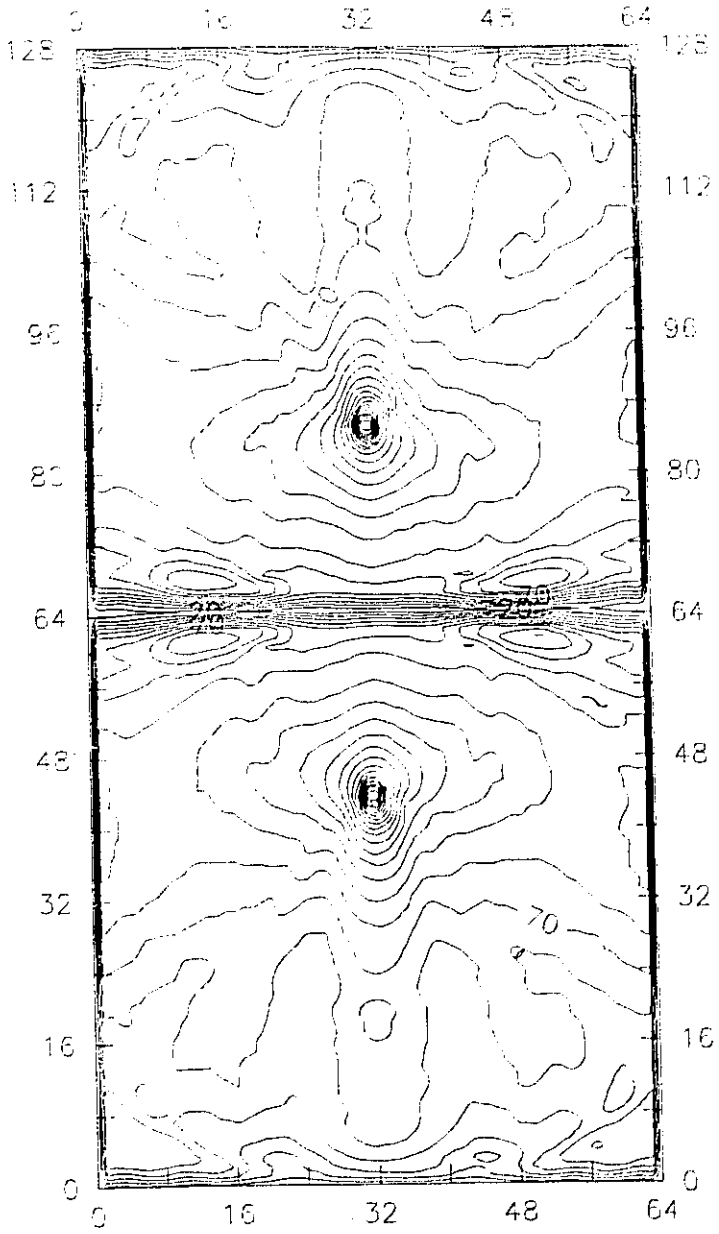

Figure 3.10: Distribution of the maximum value of the longitudinal magnetic field obtained from a reverse TLM analysis.

3.3.4 Combination of the Field Components

The observation that the transversal electric and magnetic field components both yield the contour of objects in a similar way, suggests that the difference between both fields yields a more precise image of that object. Since the particular electric field solution is maximum at the interface while the accompanying magnetic field has a local minimum at the same location, the difference between their magnitude, $|H_x(i,j)|-|E_y(i,j)|$, computed at each node, will also delimit the obstacle. Replacing by zero every negative resulting value, the obstacle will be well described. The resulting field value will thus be much lower in the empty region than close to the obstacle. Figure 3.11 illustrates the technique of processing these two field components.

Another approach is to use the magnitude of the Poynting vector, which is a combination of the three field components. Let $|P(i,j)|$ denote the magnitude of the Poynting vector.

$$|P(i,j)| = |E_y(i,j)| \sqrt{|H_x(i,j)|^2 + |H_z(i,j)|^2} \tag{3.4}$$

Taking into account what has been said about the field distribution of the different components, it can be shown that the location of the obstacle will then be described by local minima of $\left|P(i,j)\right|$. Furthermore, this approach gives a better representation of the obstacle than the local minima obtained by the transversal magnetic field only. Figure 3.12 demonstrates this. Using the algorithm that extracts the position of the local minima for each horizontal line of nodes, the shape and position of the obstacle is reconstructed with a good precision. As another example, Figure 3.13 shows a series of images including both the analysis and the reconstruction of a metallic obstacle. One can see from this example that only the left side of the obstacle is reconstructed. This is due to the fact that the induced sources have mainly be created on this side.

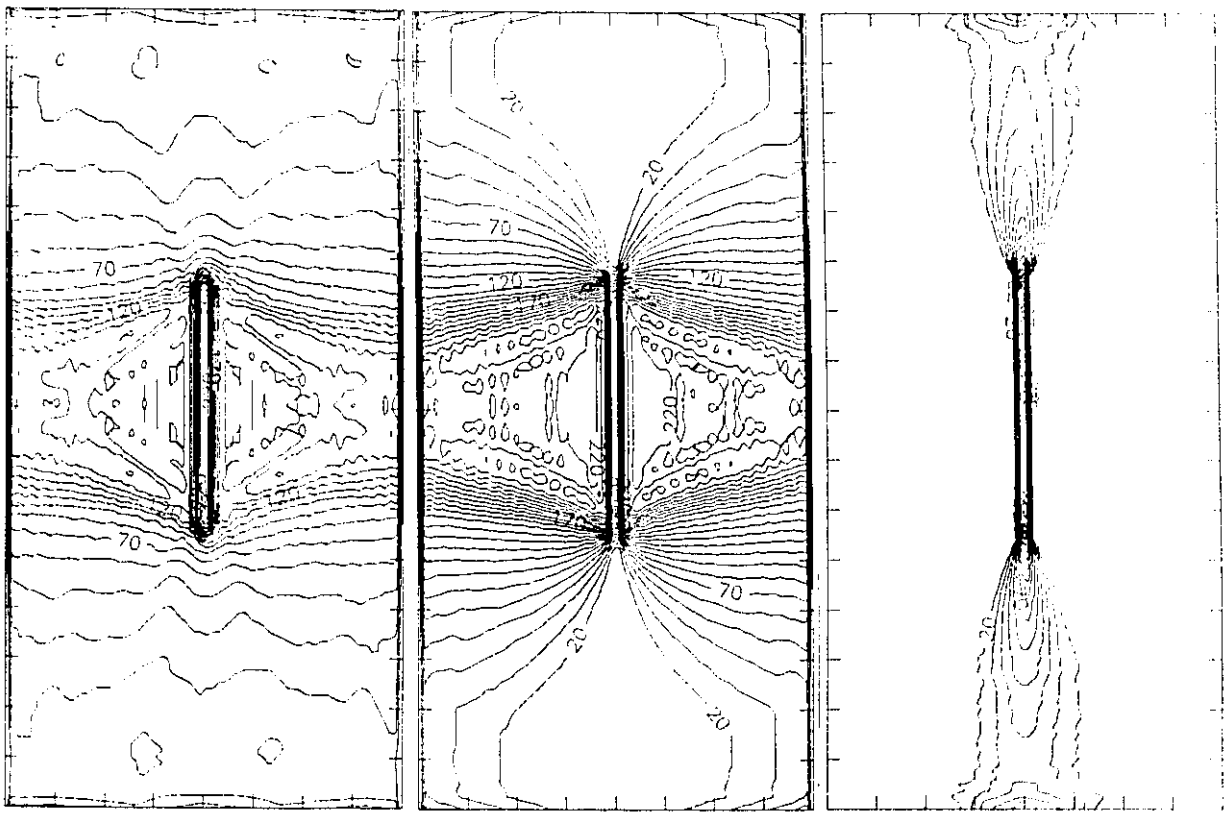

(a) (b) (c)

Figure 3.11: Comparison between the distribution of field components $|E_y|$ (a) and $|H_x|$ (b), and the difference $|E_y| - |H_x|$ (c).

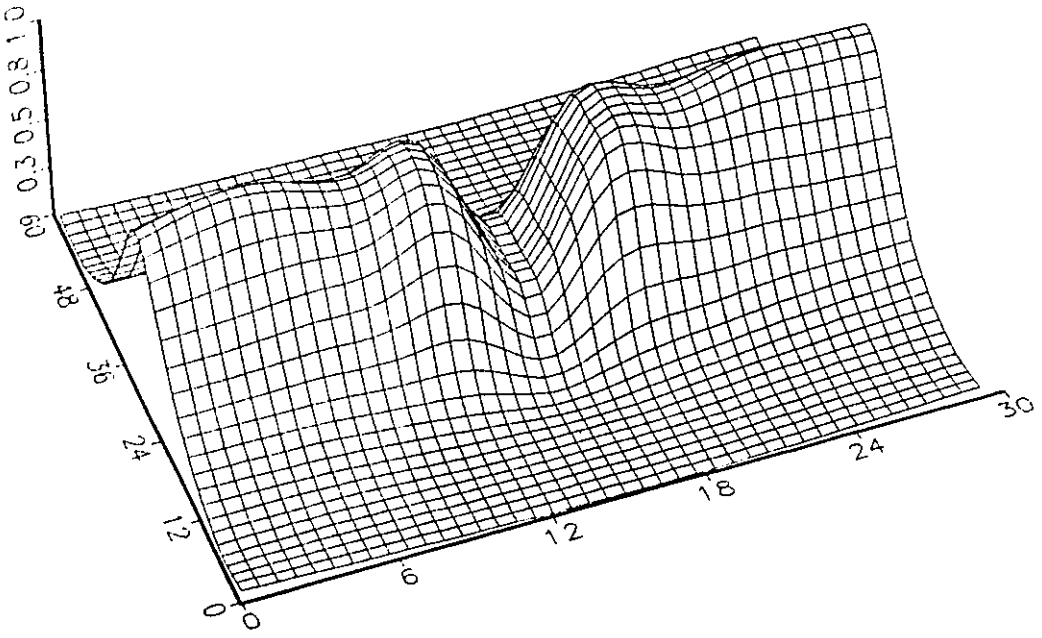

(a)

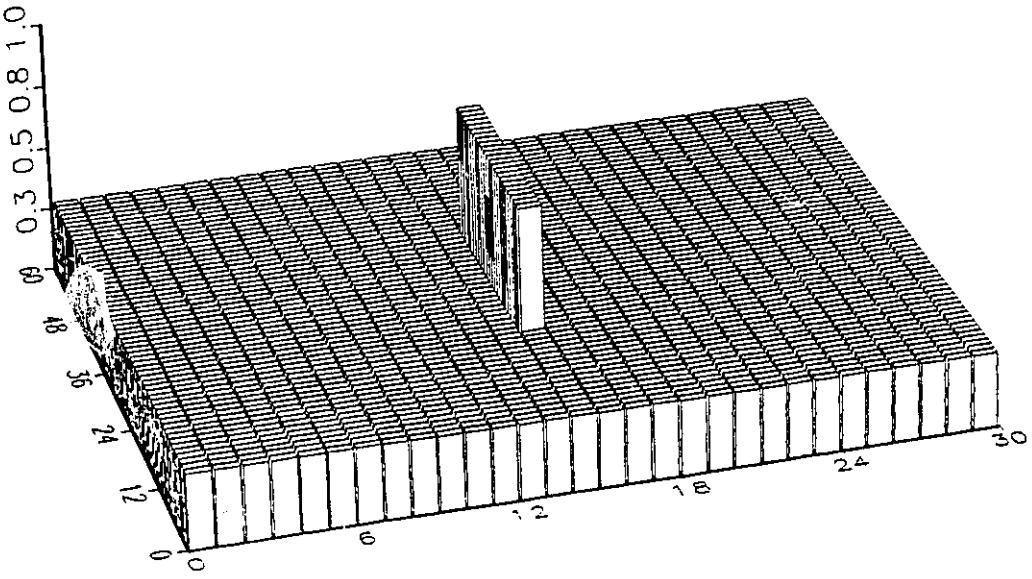

(b)

Figure 3.12: Results obtained from the display of the Poynting vector. Magnitude distribution (a) and extracted image of the obstacle (b).

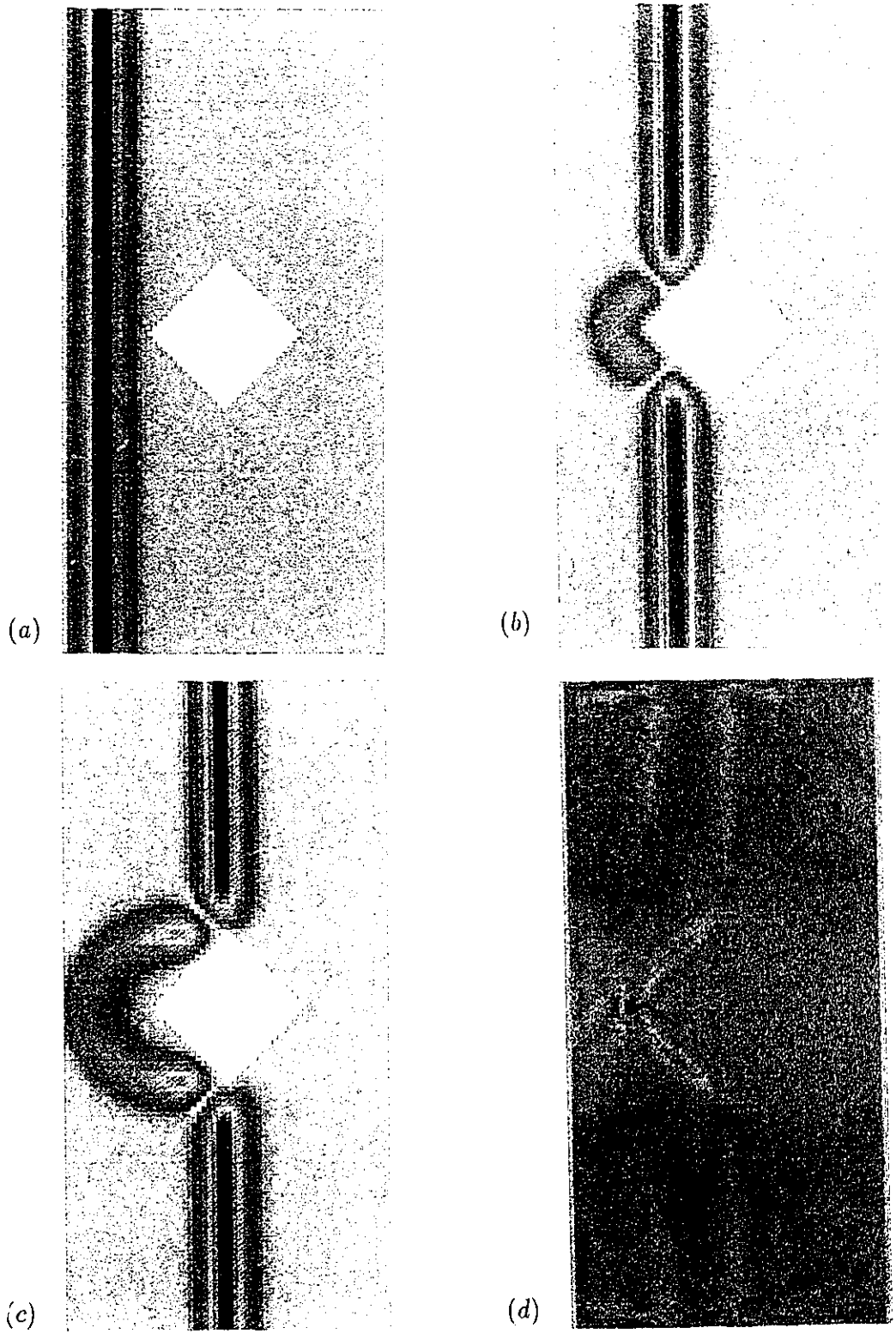

Figure 3.13: Series of images showing 3 instants during the analysis in (*a*), (*b*) and (*c*) and the result of the reconstruction in (*d*). All images display the distribution of the magnitude of the electric field component normal to the paper.

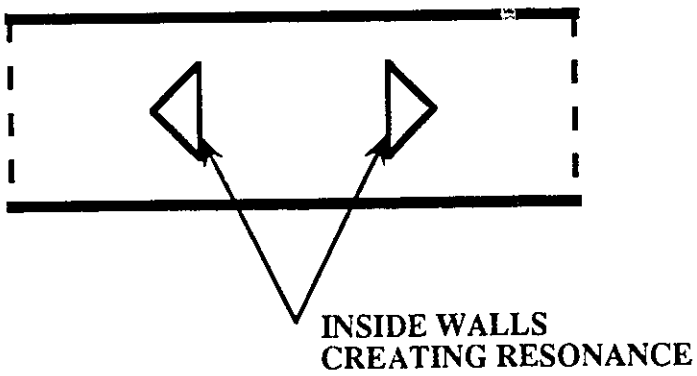

Figure 3.14: Case of the reconstruction of two obstacles having a large resonance effect between them.

3.4 Multiple Obstacle Reconstruction

So far, the reconstruction of single obstacles does not present any major problem. The examples presented above illustrate that it is easy to use the TLM method to do so. However, the extension of the shape reconstruction technique to multiple obstacles is not straight forward. Consider for example a waveguide filter which includes two metallic posts. With the TLM method, forward time-domain analysis is simple. The resonance between the two obstacles that creates the filter characteristics is taken into account in the TLM analysis. The time-domain response obtained from this analysis represents accurately the reponse of the filter. However, the application of the reconstruction technique is not simple. The information obtained at the extremities of the waveguide corresponding to the total and the homogeneous field solutions contains indirect information about the sources induced on the inside wall of the obstacle. Figure 3.14 illustrates this situation.

The induced sources created on the sides of the obstacles facing the wavefront are

directly radiating toward the absorbing boudary. The resulting information about these sources is needed to reconstruct the contour of the metallic scatterer. However, the sources induced on the inside walls of the obstacle radiate first toward the wall of the neighbouring obstacle, and before reaching one of the absorbing boundaries, the impulses travel a few times between the obstacles. This resonance effect causes the absorbing boundaries to receive only second-hand information from the inside walls of the obstacles. If the purpose of the simulation is to obtain only the frequency response of the filter, this effect is of no importance. The problem arises when the particular field solution $\phi_p(t)$ (the difference between the total and the homogeneous field solutions obtained from the two analyses) is used as a source in the inverse TLM simulation where it is expected to reconstruct the shape of the obstacle. In this case, the impulses are not able to enter into the inverse resonance for the reason that the two obstacles are not there anymore. This results in a poor reconstruction of the inside walls of the scatterers. An example of this is given in Figure 3.15; it is easy to see that the external walls are described with much better detail than the inside walls.

3.5 Shape reconstruction using the 3D-TLM condensed node

The technique described in Section 3.4 can also be applied to the three-dimensional TLM method [3, 4, 5]. In this case, a more general problem can be analysed since there is no limitation on the number of field components that can vary. With the 3D-TLM method all six field components can be computed, and the complete set of Maxwell's equations can be simulated. The use of the symmetrical condensed node provides the possibility to impose and collect all six field components at the same location in space. Figure 3.16 shows a schematic representation of a 3D-TLM

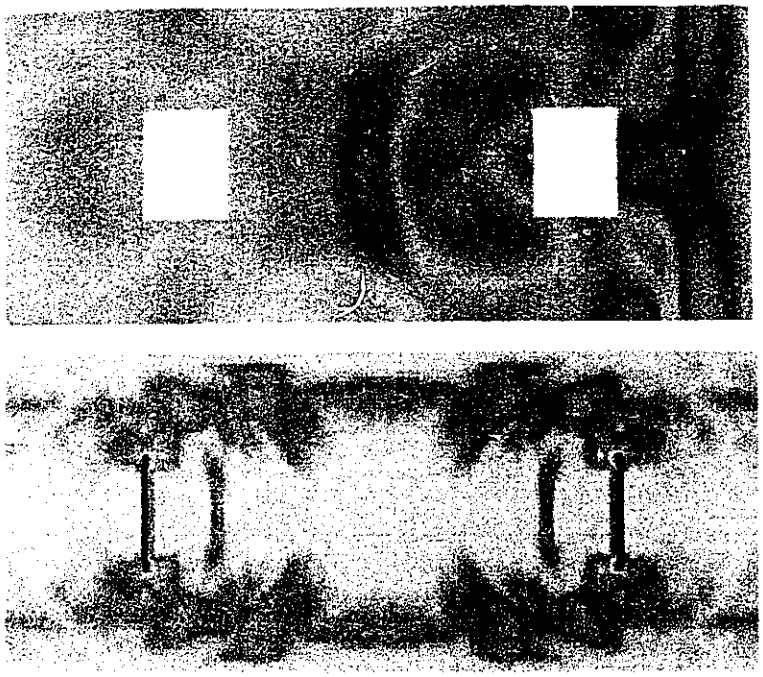

Figure 3.15: Reconstruction of two identical obstacles placed inside a parallel plate waveguide. The reconstruction of the inner walls is less accurate than the external ones.

condensed node.

As for the two-dimensional case, the study will be limited to a waveguide problem where the reconstruction of a scatterer placed in the middle of a rectangular waveguide is performed. In this 3D problem, the obstacle is not restricted to be uniform in y direction to preserve the TE_{n0} mode. In fact, it can be of any shape. The main difference with the previous case resides in the fact that instead of saving the impulses on a line at each output, the impulses emerging from the structure are now picked up in a plane on each side. Thus, a larger amount of memory is needed to save the total, the homogeneous and the particular solutions.

To illustrate the technique, a simple metallic iris centered in a rectangular waveguide will be used. Since this iris is modelled by an infinitely thin metallic wall, the lenght of the waveguide section can be relatively small compared to two other dimensions x and y. This results in a very dense mesh to describe the transversal plane of

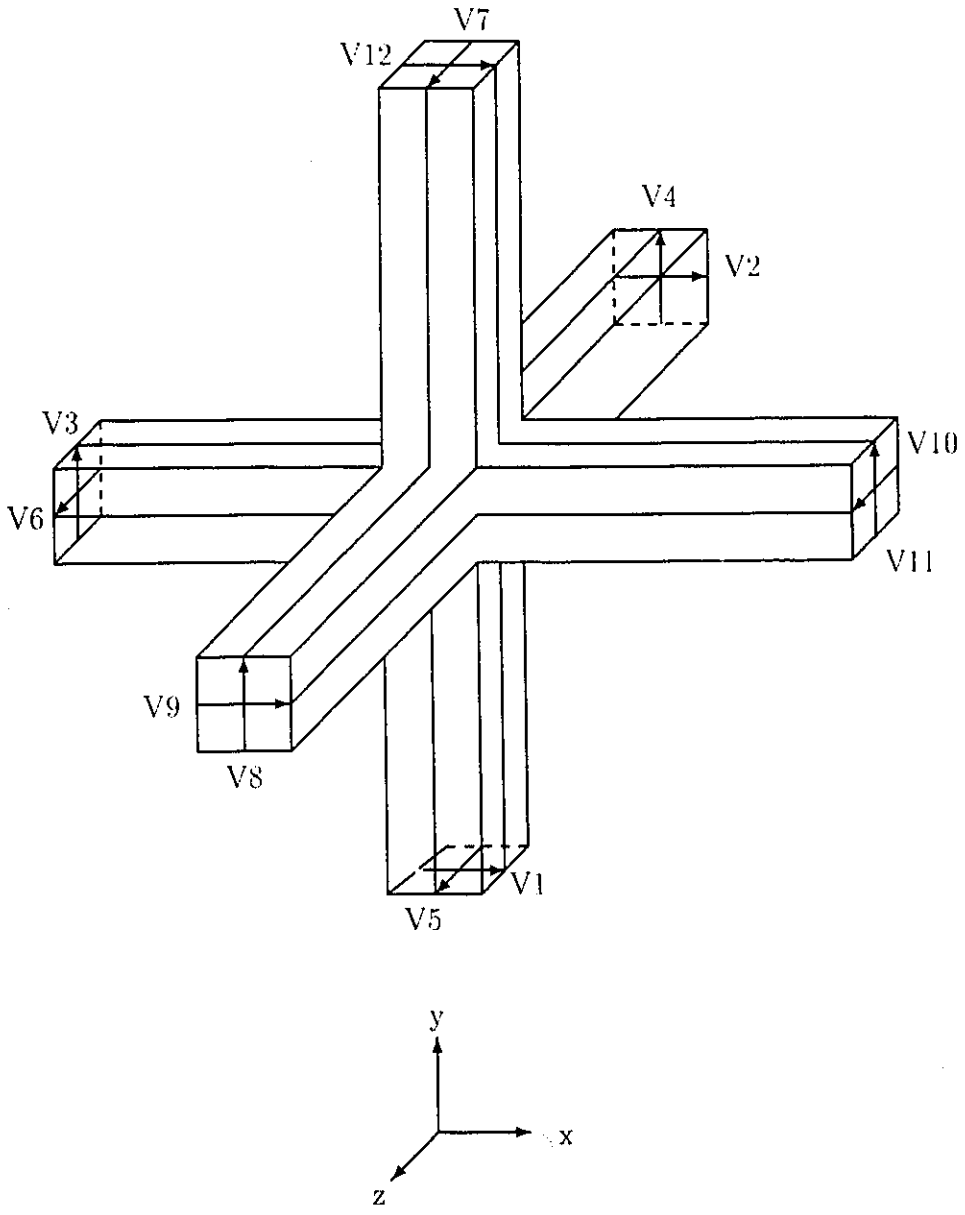

Figure 3.16: Representation of the symetrical condensed node after Johns

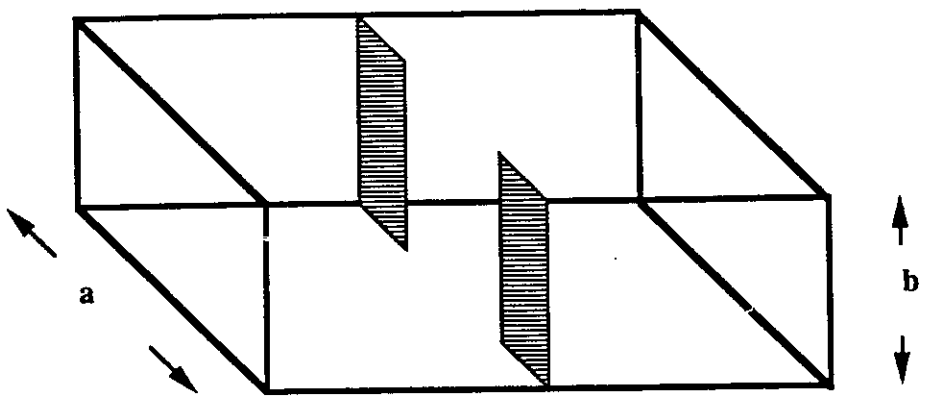

Figure 3.17: Rectangular waveguide with a metallic iris modelled with a three-dimensional TLM mesh.

the waveguide. In this way, a better description of the iris which lies in a transversal plane is obtained. The structure tested contains only a few "slices" of nodes. They each correspond to one of the $x - y$ planes in the waveguide. For the purpose of simulation, the iris is inserted between two of those slices. Figure 3.17 illustrates this modelling. Four electric walls are used to simulate the metallic waveguide walls. Furthermore, two absorbing boundaries are needed on each sides to limit the computational domain. These boundaries are located at $z = 0$ and $z = Z$ (where Z is the longitudinal dimension of the waveguide) in the TLM mesh half-way between the nodes, as in the two-dimensional case. For each node connected to the ouput planes, there are two branches corresponding to the two polarizations of the propagating wave. As can be seen on Figure 3.16 representing the symetrical condensed node, there are two orthogonal transmission-lines connecting the other nodes in each of the six directions. On the left-hand side of the waveguide, the two lines that connect to the absorbing boundary are lines 2 and 4. On the right-hand side, lines 8 and 9 are

connected to the other absorbing boundary. It is from those lines that the voltage impulses are collected in each of the two output planes. Due to the small number of nodes in the longitudinal direction, the number of iterations required for the field to vanish in the structure is relatively small. For example, in the case of the excitation of the dominant mode (TE_{10}), the wave front will have reached the right output after twice the number of nodes in the Z direction. Only some ripples due to the dispersion of the high frequency components will take more time. After propagation through 10 times the number of nodes in the longitudinal dimension, the field in the waveguide vanishes. This condition must be satisfied before re-injecting the particular solution into the empty waveguide. It is important to keep the number of iterations small since a large number of impulses must be saved at each iteration. Furthermore, the output planes being close to the scatterer, the collected impulses contain information on the higher order modes of propagation. In this way, the reconstruction of the shape of the scatterer can be performed with good resolution and efficiency.

In the case of a three-dimensional structure, the imaging of the field components is not easy. The user must select a two-dimensional plane where the field values can be converted to a color map and then displayed on the screen. For the example of the iris, by displaying the field in the transversal plane just in front of it, one can detect the shape of the metallic scatterer after re-injection of the particular response in the reverse time sequence.

Using the Connection Machine (a parallel computer), several simulations have been performed to reconstruct a simple iris. A complete example is given in Chapter 6. This example shows that the technique of shape reconstruction can be applied to the 3D version of the TLM method. It provides greater flexibility to the designer than the 2D version. The method could also be applied to other types of structures such as radiating element, for example.

Conclusion

In this Chapter, a new technique for reconstructing the shape of previously analysed obstacles has been introduced. The method is based on the time reversal property of the TLM method. Note that this technique of shape reconstruction is not a synthesis technique. However, the examples of reconstruction suggest that by specifying a wanted response, one could use the proposed technique to reconstruct the shape of an obstacle that yield the wanted reponse. The following Chapter describes the complete synthesis technique in detail.

Chapter 4

The Complete Synthesis Technique

From a practical point of view, a genuine synthesis does not start with an analysis of the wanted structure. Usually it starts with a frequency response given as a design specification. Consider an example, the specifications for a waveguide bandpass filter, where limiting values for S_{11} and S_{21} are given for a relatively narrow frequency band. Outside this bandwidth, no specifications are usually given. Furthermore, in the case of a waveguide problem, only a single mode of propagation is specified.

However, the shape reconstruction technique requires a realistic time-domain response which cannot be obtained from incomplete spectral specifications. Also, the field distribution in the transversal plane of the waveguide filter in time and space is unknown since the distribution of the energy among the different modes of propagation is also not specified. Hence, the shape reconstruction technique requires more information than is usually given in the specifications.

The missing information must be generated somehow to enable the use of the TLM method. Specifically, we must know the S-parameters over a wider spectrum and have a good description of higher order to reconstruct the topology of the scatterer with an

acceptable accuracy. In the following section, a solution to this problem is proposed.

4.1 Approximate Analysis

In the traditional synthesis techniques which involve an optimization procedure, the starting point is usually a guess or an approximate topology. This first guess is based on experience or approximate formulas. In the case of conducting obstacles in waveguides, approximate formulas exist in the literature which relates the geometry to the values of an equivalent lumped element circuit for the obstacles. The time-domain response obtained from the TLM analysis of the "first guess geometry" is then modified in the bandwidth of interest according to the specifications. Thus, the required wide frequency band information can be generated. In other words, the dominant mode response obtained from the approximated analysis (see section 4.3) is replaced by the desired (specified) dominant mode response. Thus, the signal used to synthesize the obstacle is composed of the specified response in the operating frequency range and the approximated response at the other frequencies. Usually, the original specifications are given in the frequency domain; the modification of the approximated signal is also performed in the frequency domain after a Fourier transform of the time-domain signals. Only the dominant mode time signal is converted into the frequency domain. The technique used for modifying the dominant mode response will be presented later.

4.2 Utilization of the Shape Reconstruction Technique

The modified (or hybrid) time-domain signal is used in the shape reconstruction technique as the total field solution. The homogeneous solution is subtracted from

it yielding the hybrid particular response. This response is re-injected in the reverse time sequence into the empty computational domain to yield an image of a new obstacle. This new configuration is an improved version of the approximated obstacle. Obviously, a new analysis would verify if the characteristics correspond to the specifications. A few more such cycles can be performed to achieve a good agreement between the specifications and the response of the synthetized obstacle. This algorithm converges quite fast. Experience has shown that, depending on the choice of the approximated topology, only 2 or 3 iterations are needed to achieve satisfactory results.

It is important to mention again that the specifications are compared only in the bandwith of interest and for the dominant mode. Figure 4.1 presents the flow chart of the complete synthesis procedure.

4.3 Dominant Mode Extraction

The use of a time-domain numerical method for simulating the propagation of electromagnetic waves inside a waveguide is not limited to a single mode of propagation. Even if the user has the choice of the excitation (one can excite a guide in a specific mode), higher order modes are usually generated when a wave front hits a discontinuity inside the waveguide. Depending on their cut-off frequencies and the frequency band of the excitation, these modes can be either evanescent or propagating. For example, if a WR-90 rectangular waveguide is excited by a Gaussian pulse ($\sigma = 10\Delta l$) having a half-sine distribution in the transversal dimension, the TE_{10} mode is excited. Higher order modes which are generated by the discontinuity will be evanescent. When using a time-domain numerical technique, the total time response contains all the modes, whether they are propagating or not. Thus when looking at the transversal distribution of the electric field in the waveguide, it is not possible

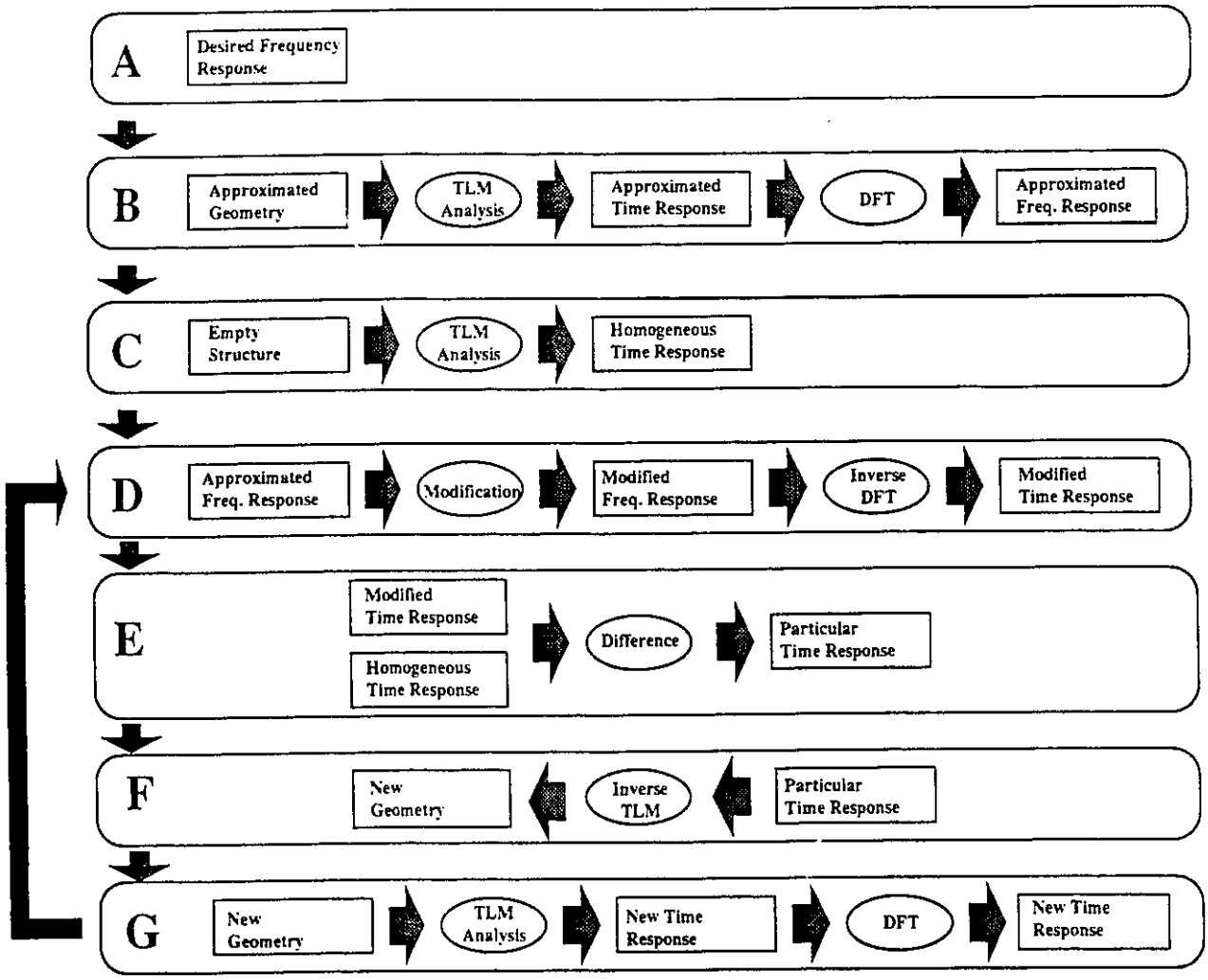

Figure 4.1: Flow chart of the complete synthesis procedure using the inversion of the TLM method (DFT = Discrete Fourier Transform).

to distinguish the different modes inside the waveguide. Only the superposition of all modes — the total field solution — is available. Since the transversal distribution of the field components of each propagating mode is represented by orthogonal functions, one can extract the magnitude of these functions by performing a Fourier expansion in the transversal plane of the waveguide. The wave that propagates inside the waveguide can be decomposed into an infinite sum of modes. For instance, the electric field distribution $E_y(x)$ in the cross section of the guide can be expanded in an infinite Fourier series as

$$E_y(x) = a_0 + \sum_{n=1}^{\infty} a_n \cos\left(\frac{n\pi x}{P}\right) + b_n \sin\left(\frac{n\pi x}{P}\right) \tag{4.1}$$

where

$$a_0 = \frac{1}{P}\int_0^P E_y(x)dx, \tag{4.2}$$

$$a_n = \frac{2}{P}\int_0^P E_y(x)\cos\left(\frac{n\pi x}{P}\right)dx, \tag{4.3}$$

$$b_n = \frac{2}{P}\int_0^P E_y(x)\sin\left(\frac{n\pi x}{P}\right)dx. \tag{4.4}$$

Each coefficient then corresponds to the relative magnitude of a mode present in the waveguide.

For the particular case of the parallel plate waveguide, the dominant TEM mode corresponds to the a_0 coefficient since this mode has a contant distribution along the x dimension. Therefore, it corresponds to the mean value of the field in transversal direction of the waveguide. Higher order mode have amplitude coefficients a_n since they will always have a cosine distribution along the x axis. Therefore, for such a waveguide, all b_n coefficients have a value of 0.

In the case of a rectangular waveguide, all a_n are zero since the conditions at $x = 0$ and $x = a$ (the width of the guide) force E_y to be zero. Thus, the field distribution in the cross-section of the waveguide is described by a sum of sine functions, and every

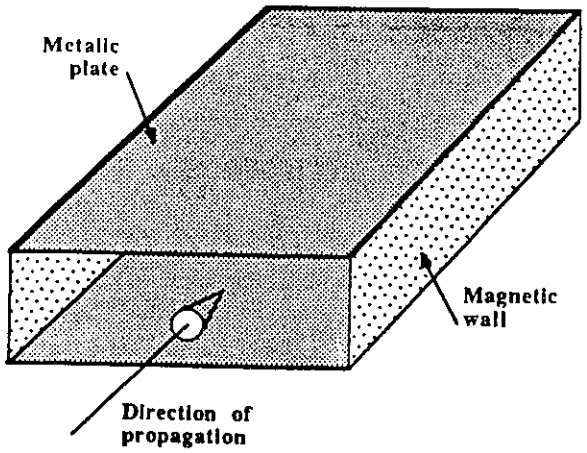

Figure 4.2: Idealized representation of a parallel plate waveguide.

b_n correspond to a mode. The TE_{10} mode can be extracted by computing the value of b_1 from Equation (4.4).

However, the fact that the responses are taken near the TEM absorbing boundary can introduce an error in the evaluation of the dominant mode response. Usually, this error is negligible in the bandwidth of interest.

let us now study the case of the parallel plate waveguide. This idealized waveguide consists of two metallic walls and two magnetic walls has shown in Figure 4.2.

When analysing the distribution of the electromagnetic fields in the cross section of such a waveguide with the two-dimensional TLM method, the boundary conditions impose a set of solutions which are orthogonal. Furthermore, when there is no disturbance in the vertical dimension, all the electromagnetic field components are constant in the y-direction, so that the only variations are along the x axis. The width a, of the waveguide is an integer multiple of the half-wavelength in transverse direction. Using the analogy with the Fourier expansion, it is possible to extract the magnitude of every mode of propagation from the coefficients of the series as mention earlier. Figure 4.3 shows the first modes of the series.

For the case of the rectangular waveguide, different boundary conditions are ap-

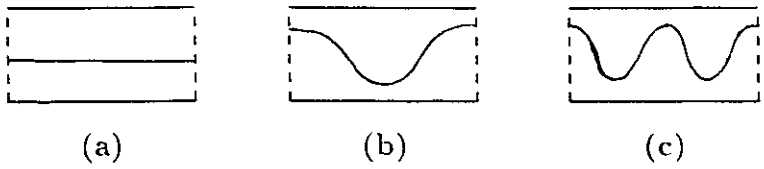

Figure 4.3: Different modes of propagations that can be seen in a two-dimensional analysis of a parallel plate waveguide.

plied since the cross-section of the guide is composed of four electric walls. The dominant mode of propagation is the TE_{10} mode which has a half-sine distribution along the x axis is constant along the y axis. The constant vertical distribution is present for every TE_{n0} mode of propagation. Only these TE_{n0} modes exist if there is no physical variation along the vertical axis inside the guide. This means that every cut along the y axis will yield an identical $x-z$ plane content. Finally, we have shown how to extract the dominant mode response of a structure. This response is then modified according to the specifications, and used with the shape reconstruction technique to provide the geometry of an obstacle corresponding to the given specifications.

4.4 Modification of the Dominant Mode Response

An important part of the TLM synthesis of microwave structures is the modification of the dominant mode information provided by the analysis of a structure with approximately the correct dimensions. The purpose of this section is to describe how to modify the dominant mode to achieve our synthesis.

In the following, it is shown how to extract the dominant mode response of a parallel plate waveguide. Let the time-domain responses for the electric field of a structure be denoted by $\phi^T_{left}(i,k)$ and $\phi^T_{right}(i,k)$. The dominant mode frequency

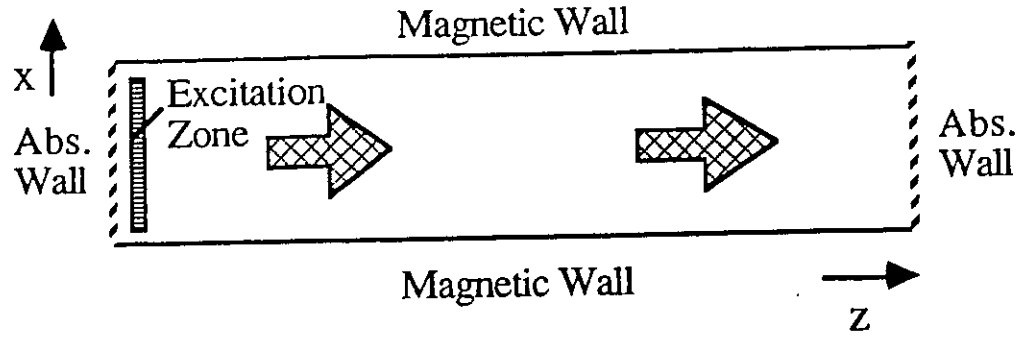

(a)

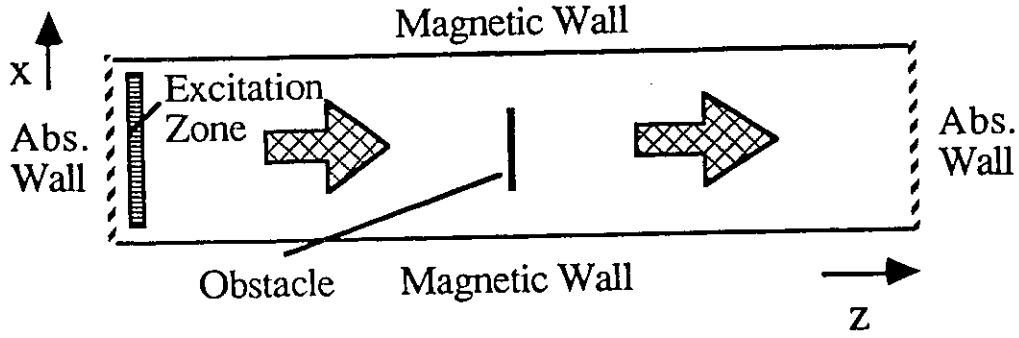

(b)

Figure 4.4: Parallel plate waveguide. (a) waveguide with an obstacle yielding the total solution (b) empty waveguide yielding the homogeneous solution.

response is extracted by performing a Fourier expansion of these signals over the transverse dimension of the waveguide at every iteration, and by taking the Fourier transform of the resulting time sequence $\phi^D_{left}(k)$ and $\phi^D_{right}(k)$. The dominant mode has a constant transversal distribution (see Fig. 4.4). Therefore, the extraction of the dominant mode is performed for each iteration by computing the average of the electric field over the x axis, resulting in the first term of the Fourier series. Hence,

$$\phi^D_{left}(k) = \frac{1}{NBX} \sum_{i=1}^{NBX} \phi^T_{left}(i.k) \tag{4.5}$$

and

$$\phi^{D}_{right}(k) = \frac{1}{NBX} \sum_{i=1}^{NBX} \phi^{T}_{right}(i,k) \tag{4.6}$$

for $k = 0, 1, 2 \ldots NbIt - 1$, where NBX and NbIt are respectively the number of nodes in the transverse direction and the number of iterations of the analysis.

Let $\Phi^{D}_{left}(\omega)$ and $\Phi^{D}_{right}(\omega)$ denote the Fourier transform of $\phi^{D}_{left}(k)$ and $\phi^{D}_{right}(k)$. Since the structure is excited from the left, Φ^{D}_{left} contains the incident and the reflected TEM wave, while Φ^{D}_{right} the transmitted TEM wave. This will be useful later.

Let the wanted frequency responses be denoted by $\Phi^{W}_{left}(\omega)$ and $\Phi^{W}_{right}(\omega)$. These are defined only for a limited frequency band where only the dominant mode can propagate. The difference between the wanted characteristics and the response of the dominant mode is obtained in the frequency domain yielding

$$\Phi^{diff}_{left}(\omega) = \Phi^{D}_{left}(\omega) - \Phi^{W}_{left}(\omega) \tag{4.7}$$

and

$$\Phi^{diff}_{right}(\omega) = \Phi^{D}_{right}(\omega) - \Phi^{W}_{right}(\omega). \tag{4.8}$$

The resulting signals contain, respectively, a reflected and a transmitted TEM wave. Therefore, the corresponding time-domain signals have a constant transversal distribution. As mentioned previously, it is easy to represent such a TEM travelling wave in a 2D-TLM network by using a line of equal node voltages with the proper incident impulses on each node. This is illustrated in Figure 4.5. If the magnitude of the electric field, A, is set to unity, then for the wave travelling to the left, the field components are calculated as follow:

$$\begin{aligned} E_y &= \frac{1}{2}\sum_i V_i \\ &= \frac{1}{2}[\frac{1}{2} + 0 + \frac{1}{2} + 1] \\ &= 1. \end{aligned} \tag{4.9}$$

$$
\begin{aligned}
H_x &= \frac{1}{Z_o}(V_4 - V_2) \\
&= \frac{1}{Z_o}(1 - 0) \\
&= \frac{1}{Z_o}, \qquad (4.10) \\
H_z &= \frac{1}{Z_o}(V_1 - V_3) \\
&= \frac{1}{Z_o}(\frac{1}{2} - \frac{1}{2}) \\
&= 0. \qquad (4.11)
\end{aligned}
$$

The resulting Poynting vector is in the $-z$ direction, and so is the direction of propagation. For a TEM wave travelling from the left to the right, we have :

$$
\begin{aligned}
E_y &= \frac{1}{2}\sum_i V_i \\
&= \frac{1}{2}[\frac{1}{2} + 1 + \frac{1}{2} + 0] \\
&= 1, \qquad (4.12) \\
H_x &= \frac{1}{Z_o}(V_4 - V_2) \\
&= \frac{1}{Z_o}(0 - 1) \\
&= -\frac{1}{Z_o}, \qquad (4.13) \\
H_z &= \frac{1}{Z_o}(V_1 - V_3) \\
&= \frac{1}{Z_o}(\frac{1}{2} - \frac{1}{2}) \\
&= 0. \qquad (4.14)
\end{aligned}
$$

Now, the Poynting vector is in the positive z direction. Therefore, for each time step k, the difference signals can be represented by a line of impulses weighted by the value of the inverse Fourier transform of $\Phi^{diff}_{left}(\omega)$ or $\Phi^{diff}_{right}(\omega)$.

Finally, the modified signals to be reinjected into the empty computational domain

that yield the shape of an obstacle according to specifications, are defined as:

$$\phi^{T'}_{left}(i,k) = \phi^{T}_{left}(i,k) - \mathcal{F}^{-1}[\Phi^{diff}_{left}(\omega)], \tag{4.15}$$

$$\phi^{T'}_{right}(i,k) = \phi^{T}_{right}(i,k) - \mathcal{F}^{-1}[\Phi^{diff}_{right}(\omega)]. \tag{4.16}$$

Using Equations (4.7) and (4.8) in (4.15) and (4.16) we obtain

$$\phi^{T'}_{left}(i,k) = \phi^{T}_{left}(i,k) - \mathcal{F}^{-1}[\Phi^{D}_{left}(\omega) - \Phi^{W}_{left}(\omega)], \tag{4.17}$$

$$\phi^{T'}_{right}(i,k) = \phi^{T}_{right}(i,k) - \mathcal{F}^{-1}[\Phi^{D}_{right}(\omega) - \Phi^{W}_{right}(\omega)]. \tag{4.18}$$

Figure 4.6 (a) shows how the two right hand side terms of Equations (4.17) and (4.18) are represented. The first terms, $\phi^{T}_{left}(i,k)$ and $\phi^{T}_{right}(i,k)$, are the total voltages of nodes i at time k resulting from the voltage impulses incident on that node. It is the total solution obtained from the TLM analysis of the structure. They contain the dominant and all the higher order modes. The second terms, which are the inverse Fourier transforms of the difference signals, contain only a TEM wave (either propagating toward the right or the left). Therefore, as mention earlier, the values of the incident impulses describing this signal are equal along the transversal dimension shown in Figure 4.6 (b) for the left input.

4.5 Conclusion

In this Chapter, a particular example has been used to illustrate how the complete synthesis technique can be applied to obtain a simple metallic scatterer inside a waveguide. It has also been shown how the missing information not included in the design specification can be generated by performing an analysis of an approximated structure.

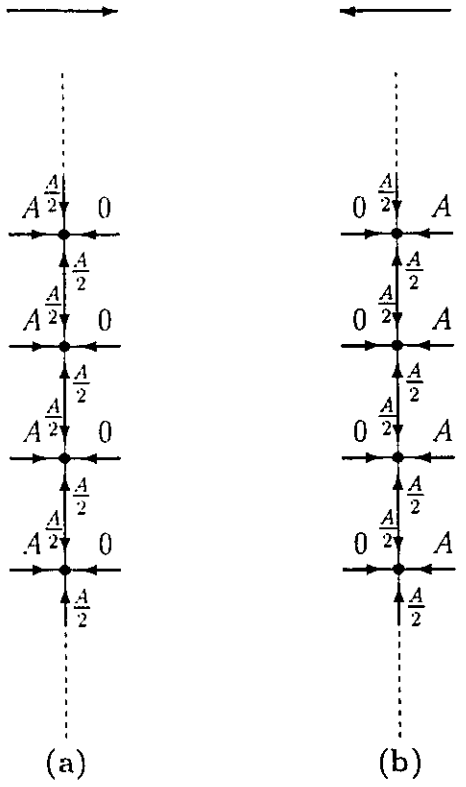

Figure 4.5: Representation of a TEM wave travelling to the right (a) and to the left (b). A is the magnitude of the electric field of the wave.

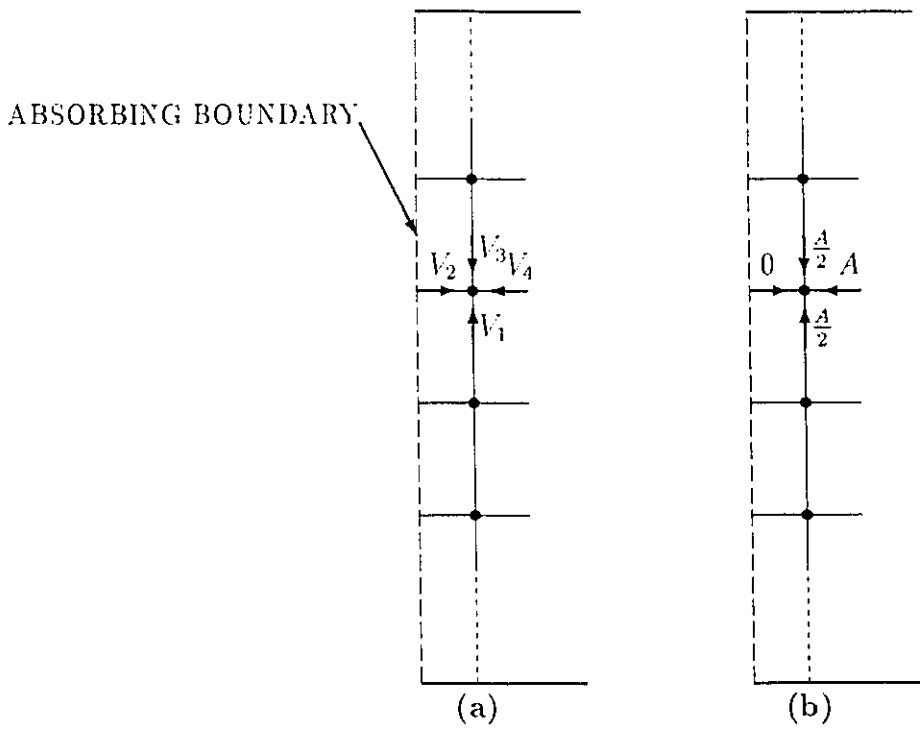

Figure 4.6: Nodes adjacent to the left hand side absorbing boundary. Voltages describing the total response (a) and voltages describing the difference signal (b).

Chapter 5

Numerical Example

In this chapter, the entire synthesis technique is presented step by step by designing an inductive obstacle inside a parallel plate waveguide.

5.1 Synthesis of an Inductive Scatterer

Suppose we want to design an inductive obstacle with an inductance of $0.9pH$, centered in a parallel plate waveguide. Using a lumped equivalent circuit (shown in Figure 5.1), the frequency domain characteristics are computed. The scattering parameters S_{11} and S_{21} of the inductance are shown in Figure 5.2 vs the normalized frequency $\Delta l/\lambda$. Recall that these curves are valid only in the single-mode frequency band and for the dominant mode of propagation.

At this point, the designer must choose an approximated structure among several possible geometries which could satisfy the requirements. The obstacle could be, for example, a circular or a rectangular post, a thin iris or a thin transversal septum. We choose the latter for the simplicity of the analysis.

As mentioned in the previous chapter, this geometry is used to generate an approximated wide frequency band response which includes the higher order modes of

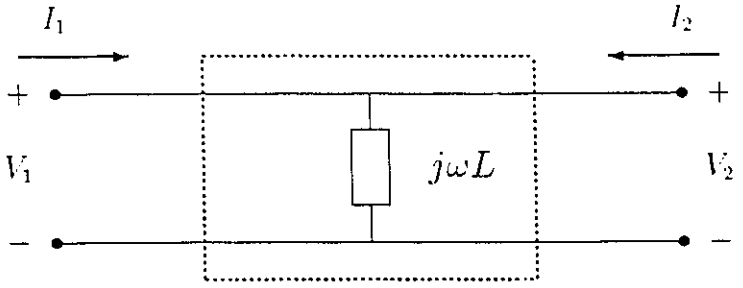

Figure 5.1: Shunt inductance of $0.9pH$ which is used to generate the specifications for the design.

propagation. To illustrate the convergence of the procedure, we set the first guess width of the transversal septum arbitrarily to $41\Delta l$. The 2D-TLM mesh describing the guide contains 29 by 100 nodes. Magnetic walls are used to simulate the sides of the parallel plate waveguide, and two TEM absorbing boundaries are used to limit the computational domain. The absorbing boundaries are made of single reflection coefficients which can absorb a TEM plane wave. Figure 5.4 shows the exact dimensions of the approximate structure.

The TLM analysis of this structure is performed to obtain an approximated response. As in the shape reconstruction technique, all the impulses incident upon the absorbing boundaries are saved to yield to total field solution $\phi^T_{right}(i,t)$ and $\phi^T_{left}(i,t)$. From these, the dominant mode time-domain response is extracted. Then, using a discrete Fourier transform, the frequency domain response is obtained. Finally, using the technique for the extraction of the scattering parameters presented in the chapter 2, $S_{11_{app}}$ and $S_{21_{app}}$ are computed. These approximated scattering parameters are shown in Figure 5.5.

The obtained response must be modified according to the design specifications. In the current bandwith of interest, between 0 and 0.01 $\Delta l/\lambda$, the approximated scattering parameters are replaced by the scattering parameters of the $0.9pH$ induc-

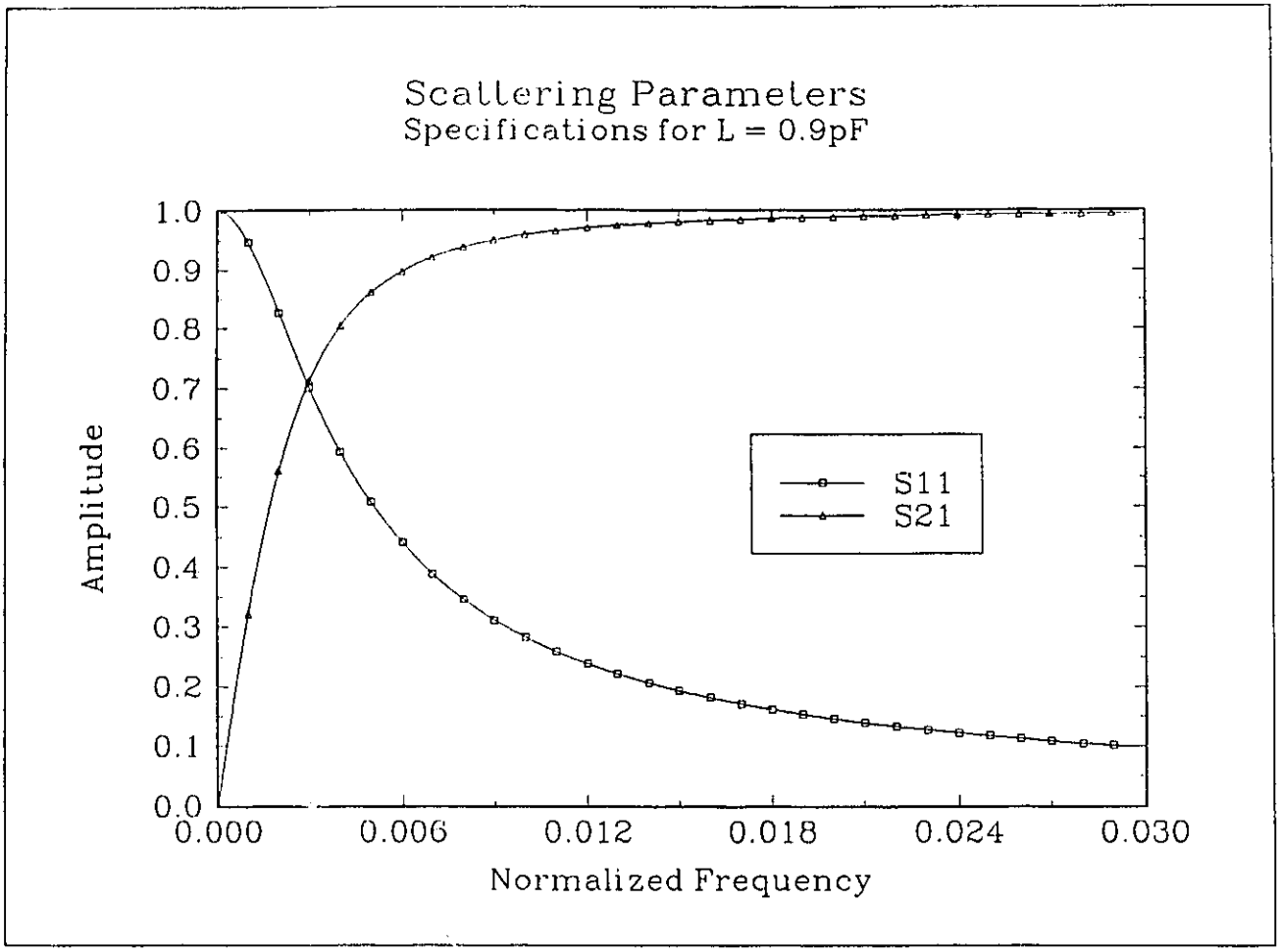

Figure 5.2: Scattering parameters S_{11} and S_{21} of an inductance of $0.9pH$. These are the design specifications for this example.

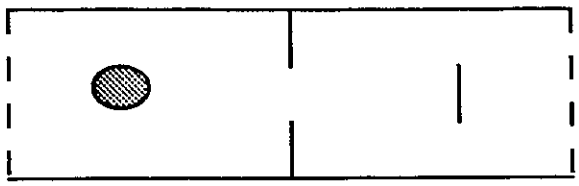

Figure 5.3: Several possible obstacle cross-sections which can approximate the design characteristics of the shunt inductance.

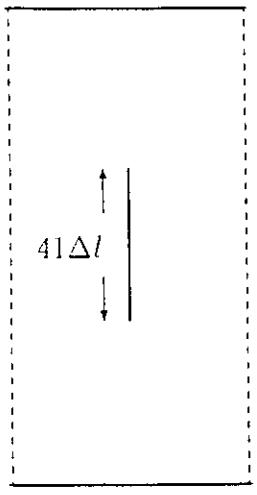

Figure 5.4: Appoximate structure.

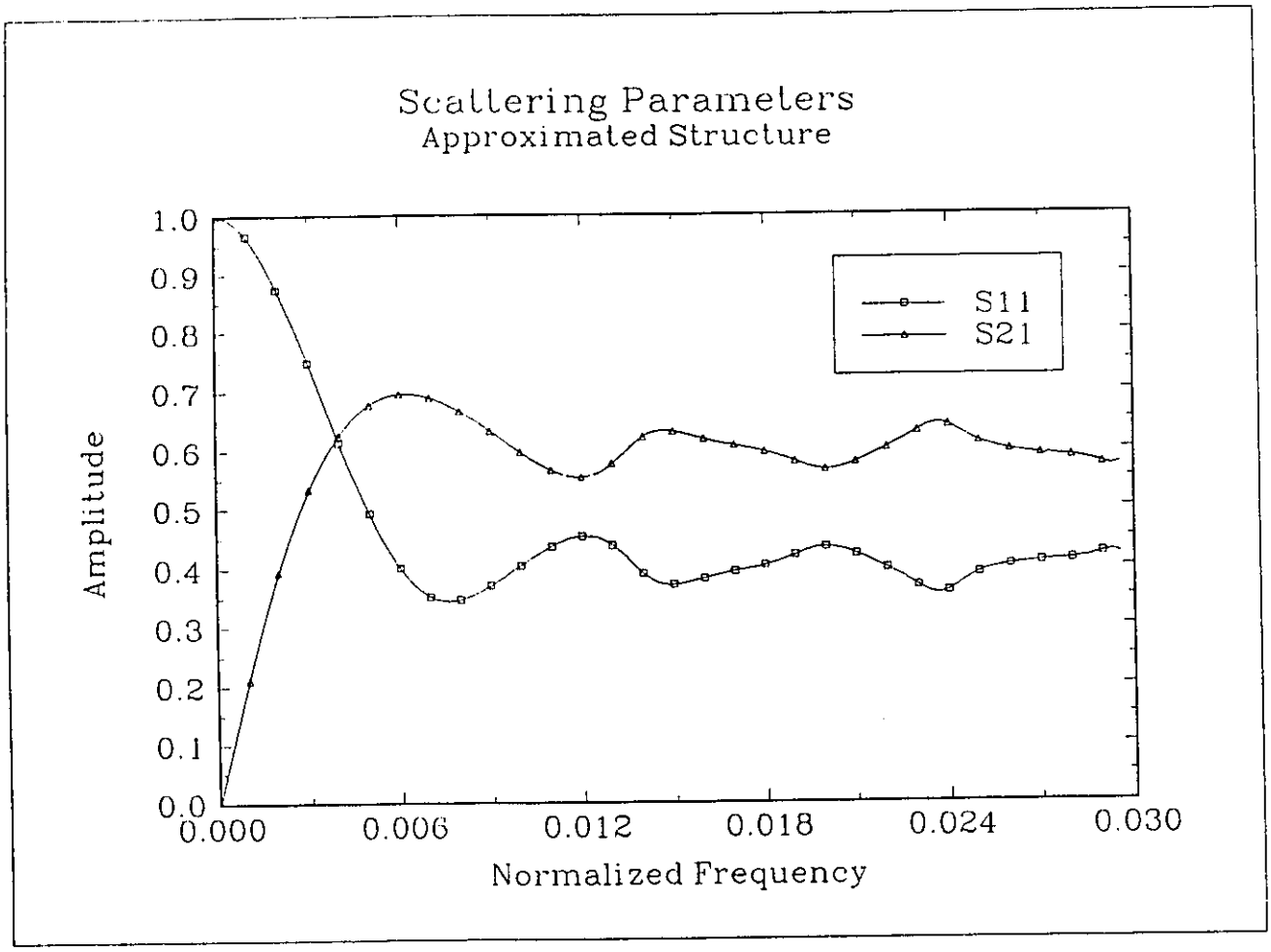

Figure 5.5: Scattering parameters obtained from the TLM analysis of the approximate structure. They represent the frequency domain response of the dominant mode.

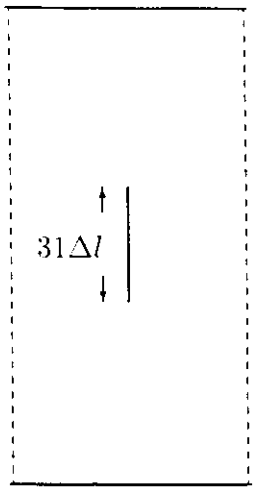

Figure 5.6: New configuration.

tance. This results in a hybrid frequency response which corresponds partially to the approximated structure and to the wanted inductance.

The hybrid response is used as the new total field solution in the shape reconstruction technique. Prior to re-injecting the new total field solution into the empty computational domain in reverse time sequence, the difference between this new response and the homogeneous response is computed.

From the backward simulation, a new configuration is extracted. It can be seen that it is an identical structure having a width of $31\Delta l$. Figure 5.6 shows this new configuration. To verify its validity, a new TLM analysis of this obstacle is performed. The resulting dominant mode response is given in Figure 5.7.

From these responses for S_{11} and S_{21}, we can see that the design requirements are almost satisfied. Another iteration would give more accurate results. Depending on the required accuracy, the process may be stopped here.

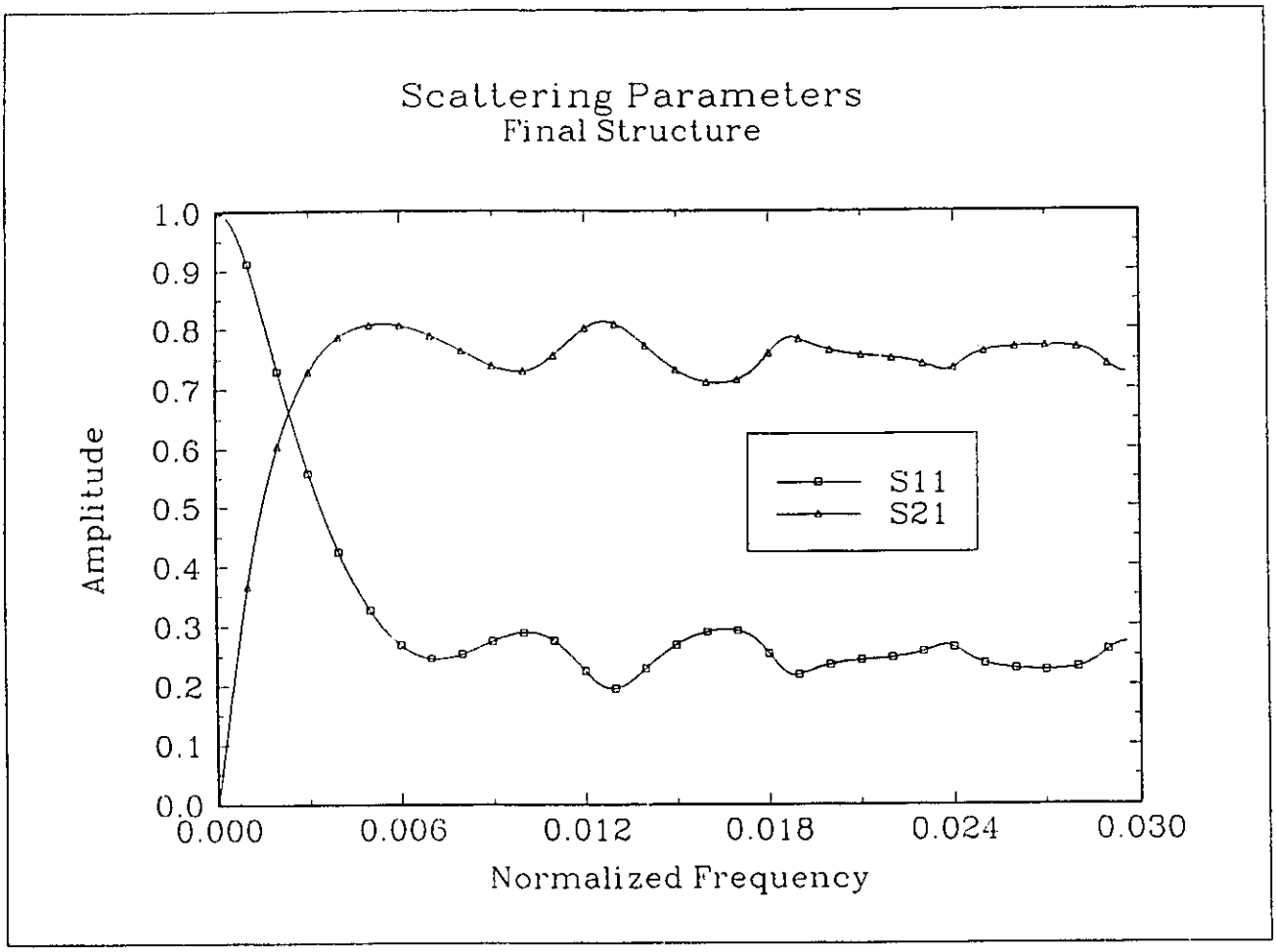

Figure 5.7: Scattering parameters of the new configuration. The low frequency part already corresponds to the design specifications.

5.2 Conclusion

In this Chapter, the new time-domain synthesis technique has been completely illustrated using the design of an inductive obstacle as a simple example. The size of a thin septum has been computed in only a few iterations. Results have shown that for this case, acceptable results where obtained in a single iteration.

Chapter 6

Parallelisation Using the Connection Machine

An important part of the work for this thesis has been performed in collaboration with Le Laboratoire d'Électronique of the Université de Nice — Sophia Antipolis in France. Professor Albert Papiernik, director of the laboratory authorized the use of the laboratory facilities for four months, including the acces to a Connection Machine, a massively parallel computer.

During this period, I was able to test the synthesis technique on this supercomputer since the Transmission-Line Matrix method is easy to implement on it. It has resulted in a major reduction in computer time for most of the simulations. In this chapter, the essential results from this work in France are reported.

6.1 The Connection Machine

The Connection Machine is a parallel computer built by the Thinking Machine Corporation, which has a large number of very small processors. All the processors can communicate with each other with high speed. However, the connections between

them is controlled by the software. This means that the processors can be configured in such a way that it fits the TLM mesh under study. Therefore, the Connection Machine is a very powerful and flexible tool for TLM modelling.

The hardware of the Connection Machine consists of a few sets of processors. Each set is composed of 8192 processors. Each processor is operating only on one bit. This explains the high number of processors in a set. These can be combined to obtain a supercomputer of 64 thousands processors. The memory is also divided in parallel parts. Segments of 256k Bytes are attached to every processors. Also, a parallel disk that provides the ability to store very large parallel files with a direct acces from the processors, is connected to the system.

For the user interface, the Connection Machine is accessed from a Unix workstation. The commands to operate the Connection Machine are given from this front-end computer. From the user point of view, the Connection Machine looks like a standard Unix system. Only a few new commands are needed to operate it.

To operate the Connection Machine, two major languages are available (in addition to the basic parallel assembly code). The more often used is the CMFortran, a special Fortran language which is adapted to the Connection Machine. Also, there is the C* (C star), which is an improved version of C++, that includes a series of functions and operators needed to create and use parallel variables. The C* language has been chosen to do the work since the TLM simulator was written so far in C language. Therefore, the conversion to a parallel version was simplified.

6.2 The Parallel TLM Algorithm

The Transmission-Line Matrix method has been used so far almost exclusively on sequential computers. The algorithm was initially developed for such a computer structure. The computation for updating the node voltage is done at each time step

sequentially for each node in the structure. From one node to the next, only the voltage impulse values change, but the computation is identical. The computation has to be done at every nodes one at the time. This results in a large computation time. By performing the identical computation on all nodes simultaneously for each time step, it is possible to reduce by a large factor (the number of nodes) the CPU time required to do a given TLM computation. To this end, each available processor is associated with a TLM node, and the basic scattering is performed at every node simultaneously. The memory associated with each processor contains the respective values of the impulses incident upon the node.

The simulations described in this thesis where done on the Connection Machine. The computation time has been improved by a factor of almost 20, depending on the situation. After executing the parallel version of the TLM synthesis program, the following points where observed.

- The TLM computation time on the Connection machine is improved. However, the reduction in CPU time is lower than expected. The synthesis technique requires writing and reading on the disk the values of the impulses incident on both absorbing boundaries at every iterations. This usually takes more time than the TLM computation itself. Table 6.1 shows some results comparing the sequential and the parallel execution time with and without disk writing.

- The reduction in CPU time increases with the number of nodes. In fact, there is no major difference between the sequential and the parallel computional time if only a few nodes are needed to describe the structure.

  For example, let n denote the number of operations to be performed on p processors (or nodes). If each of these operations takes a CPU time t, then the idealized sequential computation time T_s required is given by:

$$T_s = npt. \tag{6.1}$$

However, the parallel CPU time T_p required to perform the same task is:

$$T_p = nt. \tag{6.2}$$

Hence, the improvement given by the ratio r of the sequential and the parallel CPU time is:

$$r = \frac{T_s}{T_p} = p. \tag{6.3}$$

As one can see, the improvement on the computational time is directly proportional to the number of nodes in the TLM mesh. Therefore, the use of a parallel computer such as the Connection Machine is more efficient for a large number of nodes. Unfortunately, this improvement is reduced by the aspect of the communications between the nodes. The ratio r depends also on the communications which slow down the speed of the computation. The comparisons mentioned above only show the effect of the number of nodes on the increase of computer time.

- Finally, all the scalar variables (as opposed to the parallel variables) are handled by the front-end computer. The use of scalar variables reduces the parallelization factor which, in turn, tends to reduce the speed of the computation. This is due to the slow communications between the Connection Machine and its front-end computer. Every time the program needs a scalar variable, the control is transferred to the front-end computer. This makes the overall computational time larger. By reducing the access to the front-end computer, it is possible to reduce this effect.

6.3 3D-version of the TLM Program

Some experiments have been performed on the Connection Machine using the 3D condensed TLM node. The purpose was , in fact, to investigate the possibility of

Description of the simulation	Computation time: sequential	Computation time: parallel
8192 nodes 1500 iterations	301 sec	195 sec
8192 nodes 1500 iterations Minimization of the scalar variables	301 sec	18 sec
16384 nodes 1500 iterations Minimization of the scalar variables	600 sec	20 sec
8192 nodes 1500 iterations Saving of the impulsions at the outputs	445 sec	30 sec

Table 6.1: Results comparing TLM simulations on a DEC 5500 computer and on the Connection Machine.

applying efficiently the TLM synthesis technique to a 3D problem.

6.3.1 Data Structure

The investigation has been restricted to the problems of thin obstacles inside rectangular waveguides. Furthermore, due to the restrictions on the arrangement of the processors, which impose a number of nodes equal to a multiple of 8192, and each dimension to be a multiple of 2. Figure 6.1 shows the waveguide geometry chosen. The dimensions used for this problem were $128 \cdot 64 \cdot 8 = 65536$. This data structure format gives a very good resolution in the $x - y$ plane. Also, since the guide has a short length, the number of iterations required until the field vanishes in the guide is reduced. Moreover, the proximity of the reference planes to the obstacle provides a good description of the higher order modes.

The most important difference between 2D and 3D problems concerns the saving of the impulses at both ends of the waveguide. In the 3D case, emerging impulsesmust be stored for a plane rather than a line of nodes. This increases considerably the amount of memory storage required for the reconstruction of the obstacle. Furthermore, there is the problem of the absorbing boundaries for the 3D TLM mesh. In this experiment, a single reflection coefficient has been used to terminate the lines in the absorbing planes. This introduces some errors in the impulse reponses extracted from the structure but does not influence the precision of the reconstruction. A wideband dispersive absorbing boundary condition would give more accurate results.

6.3.2 Results

Figure 6.3 shows some results of the reconstruction of an inductive iris inside a rectangular waveguide. The display shows the distribution of the magnitude of the electric field in the cross section of the guide. Figure 6.3 (a) shows the distribution of the

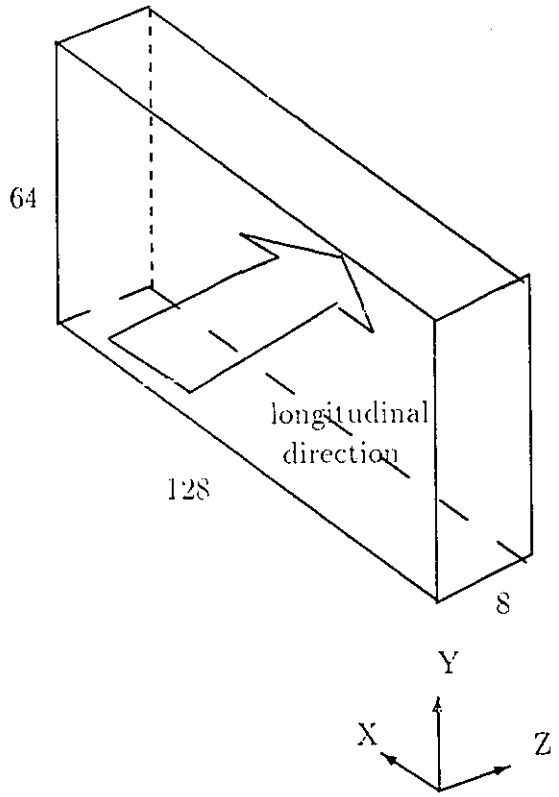

Figure 6.1: Waveguide structure as simulated using the Connection Machine. Dimensions are given in Δl.

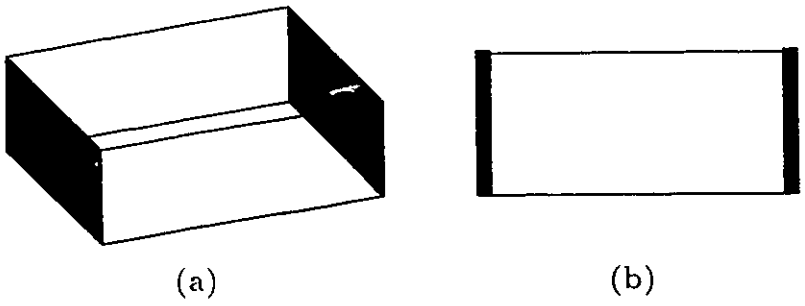

Figure 6.2: Comparison between the information to be stored in a 3D (a) and a 2D (b) TLM synthesis problem

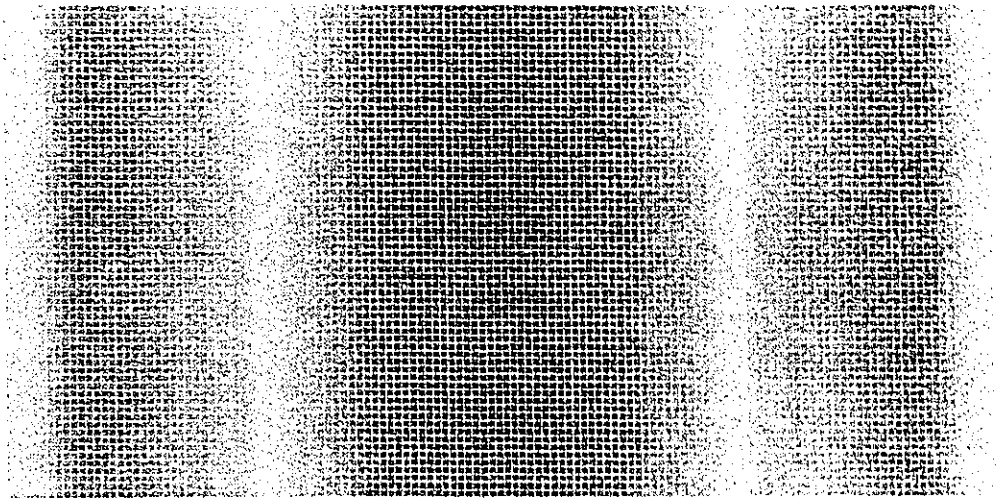

(a)

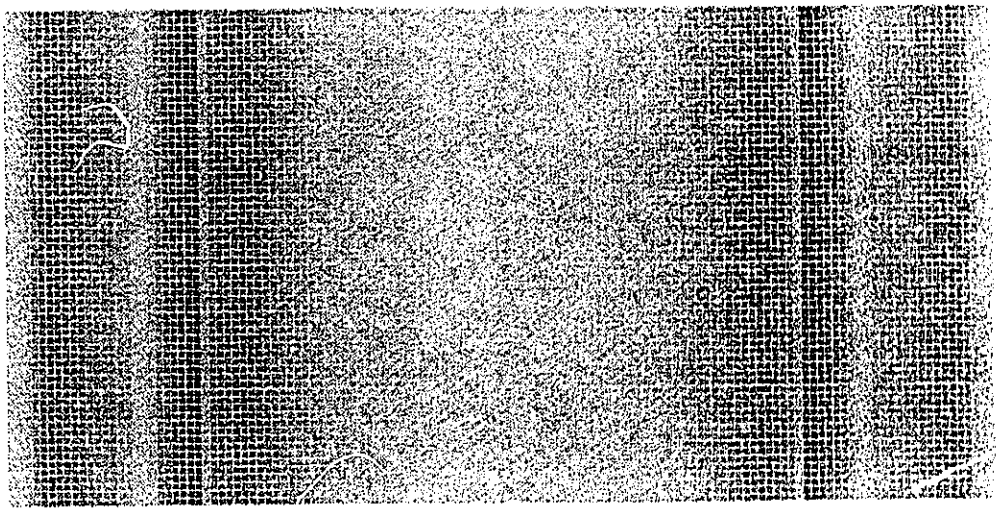

(b)

Figure 6.3: Example of reconstruction of a thin iris in a rectangular waveguide. The distribution of the magnitude of the electic field in the cross section of the guide is shown.

electric field inside the guide without the metallic obstacle. It is easy to recognize the half-sine distribution of the field in the guide. In (b), the distribution of the field for the reconstructed iris is shown. The edges of the iris are localized by the highest values of the field. These are indicated by the brightest red lines. The obstacle can be easily reconstructed with very good precision.

Althought the computation is straight forward, the problem of visualizing the field components in a three-dimensional space is an important one. Good results for the reconstructions were obtained only for some thin obstacles. For complex objects, a complicated processing of multiple images should be used. Therefore, only simple structures were tested. On the other hand, since the display used in the reconstruction lies in the $x-y$ plane, it gives a very good resolution in that plane. This makes possible the reconstruction of irises of any shape in that plane, as can be seen in Figure 6.4.

Numerical experiments were performed on the synthesis of thin irises from the modified responses obtained from the TLM analyses. Some observations must be mentioned here. First, the extraction of the dominant mode response is different from the 2D case. Now, the dominant mode is the TE_{10} mode. It corresponds in the Fourier expansion to the first term of the sine series rather than to the constant term as in the case of the TEM mode. Hence, the equation

$$E_{TE}(t) = \frac{2}{NBX} \sum_{i=1}^{NBX} \left(\frac{1}{NBY} \sum_{j=1}^{NBY} E(i,j,t) \right) \sin\left(\frac{\pi(i-0.5)}{NBX} \right) \qquad (6.4)$$

is used to extract the amplitude of the electric field.

From this time-domain signal, one can extract the frequency domain signal which must be modified according to the design specifications. Exactly the same technique as for the 2D case can be applied. The only problem resides in the CPU time needed to extract the dominant mode information in the time domain. This operation requires the access to the parallel disk, which is relatively slow from the front-end computer. Since the resulting time-domain signal is not a parallel variable, it consumes a large

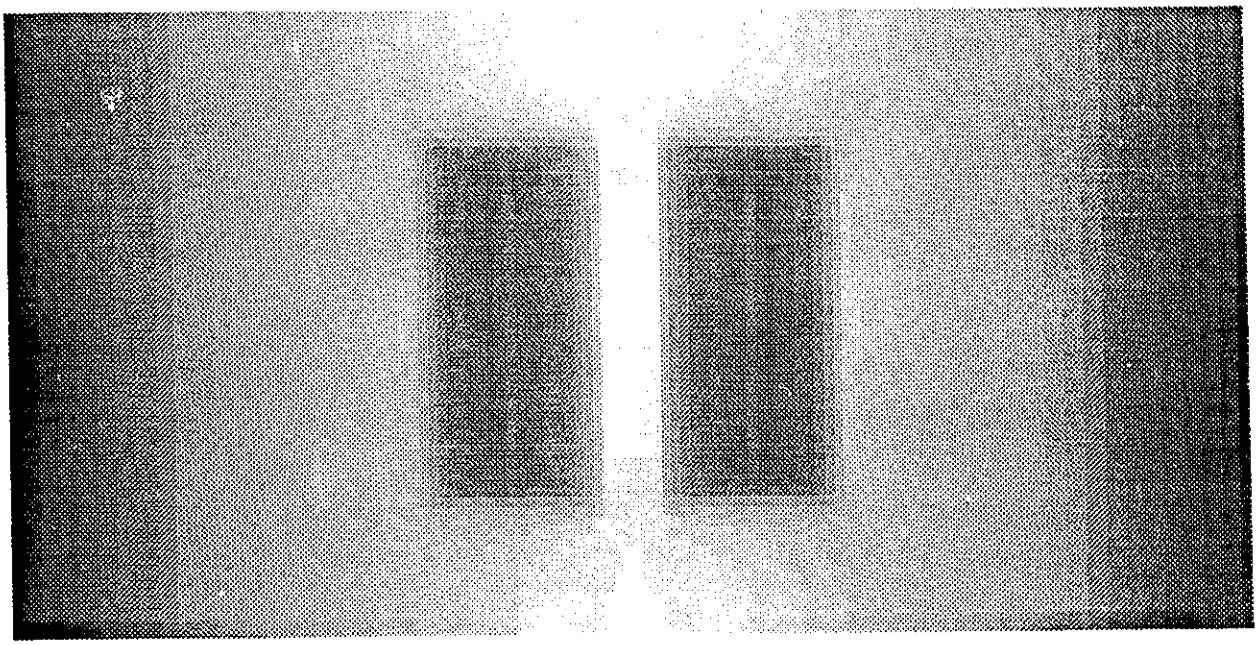

Figure 6.4: Example of reconstruction of a thin iris in a rectangular waveguide. In this case, the obstacle is a conducting plate which has two rectangular holes. Distribution of the magnitude of the electic field in the cross section of the guide. Light grey indicates the highest values of the field.

amount of time. Figure 6.5 illustrate this conversion process.

6.4 Conclusion

The TLM synthesis technique has been implemented on a massively parallel computer. This has resulted in a large reduction of the computation time. However, even if the conversion of parallel to sequential data is not as efficient, the parallelization still provides a respectable improvement for the TLM synthesis computation. Further improvements could be introduced to accelerate the overall process. Among others, the parallel implementation of the time and frequency domain response processing would accelerate the execution.

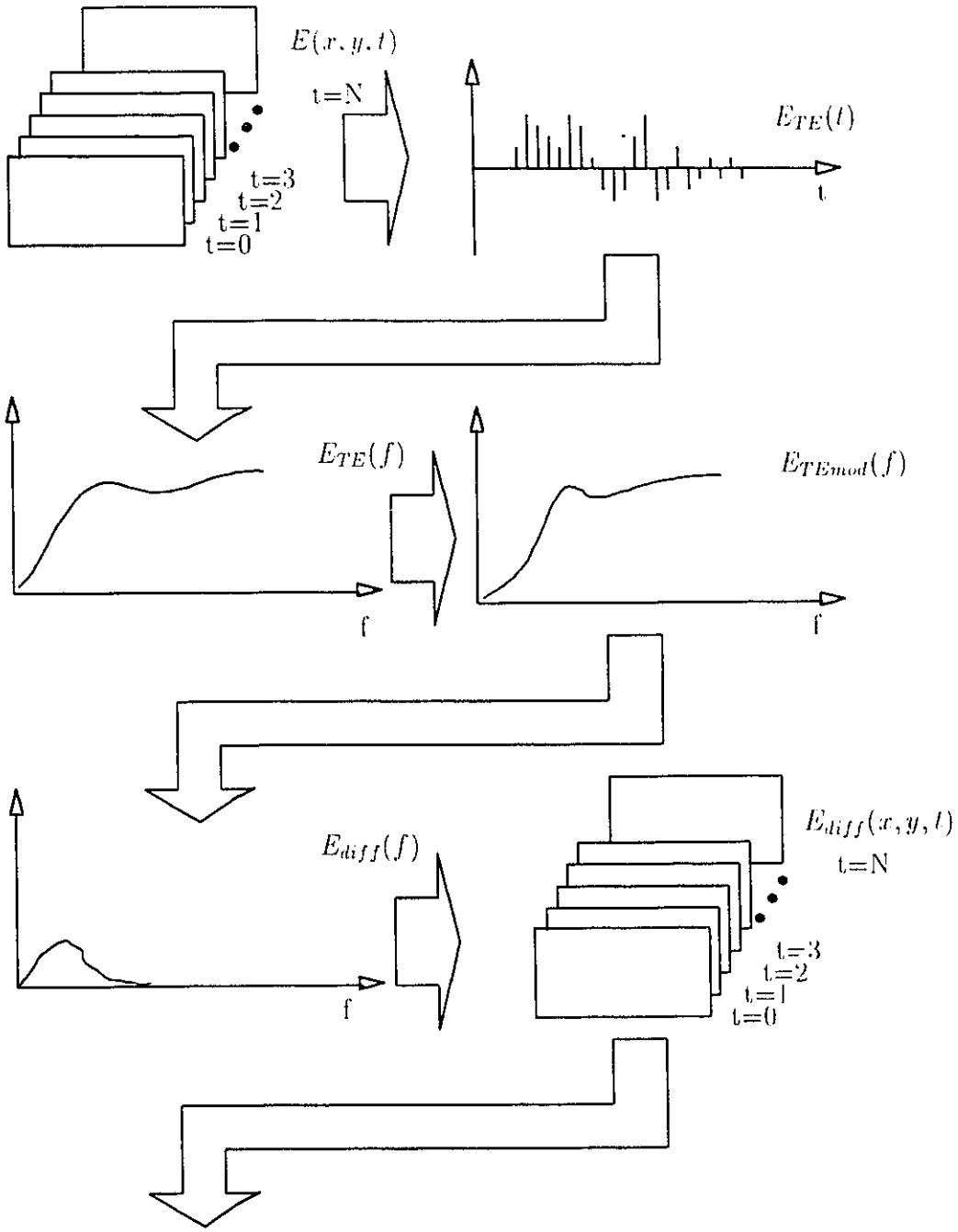

Figure 6.5: Diagram of the modification of the response obtained from a 3D-TLM analysis.

Chapter 7

Conclusions

In this thesis, a novel technique for the time-domain synthesis of metallic scatterers has been presented. It is based on the time reversal property of the Transmission-Line Matrix method. It has been shown that by alternating between forward and backward analyses, it is possible to reconstruct the shape of a previously analysed obstacle. It has also been shown how the high frequency information mission from the design specifications can be generated by analysing an approximated topology of the structure.

Applications of this technique are possible in many fields of microwave technology. Among these are the design of discontinuitites, matching circuits of planar structures and rectangular waveguides. It may also be applied to the design of antennas in order to obtain, for example, the shape of a printed antenna corresponding to a specified input impedance.

Further research should be carried out in the synthesis of multiple obstacles since most practical microwave devices contain more than one discontinuity.

The possibility of combining image processing with this technique is also a topic of further reaserch. It might improve the overall efficiency by reducing the density of nodes required for an accurate reconstruction of the obstacle. Some recent devel-

opment in signal processing could be used to reduce the number of TLM iterations necessary to obtain a satisfactory frequency domain responses.

Also, the TLM algorithm is advantageously implemented on a parallel computer. A large reduction of the computational time can be achieved when using the Connection Machine.

Finally, the technique is still young and promissing. Much work is needed to extend its application to other types of structure and to reach a level of pratical usefulness.

Bibliography

[1] R. Sorrentino, P.P.M. So, W.J.R. Hoefer, " Numerical Microwave Synthesis By Inversion Of The TLM process", in 21^{st} *European Microwave Conference Digest*, pp 1273-1277, Stuttgart, Germany, Sept. 1991.

[2] P.B. Johns, R.L. Beurle, "Numerical solution of 2-dimensional scattering problems using a transmission-line matrix", *Proc. Inst. Electr. Eng.*, vol. 118, pp. 1203-1208. Sept. 1971.

[3] W.J.R Hoefer, " The Transmission-Line Matrix Method - Theory and Application", *IEEE, trans. Microwave Theory Tech.*, vol. MTT-33, pp. 882–893, Oct. 1985.

[4] W.J.R. Hoefer, "The Transmission-Line Matrix", Chapter in *Numerical Technique for Microwave and millimeter-wave Passive Components*, John Wiley, 1989, London.

[5] W.J.R. Hoefer, P.P.M. So, "The Electromagnetic Wave Simulator", John Wiley, 1991, London.

[6] W.J.R. Hoefer, "The Discrete Time Domain Green's Function or Johns Matrix — a New Powerful Concept in Transmission Line Modelling (TLM)", *International Journal of Numerical Modeling*, Vol.2, pp.215-225, 1989.

[7] Y. Uher, W.J.R. Hoefer, "Evaluation of Scattering Parameters Using the 3D-TLM", Conference Digest, International Microwave Symposium, IEEE MTT-S, Dallas TX, 1990.

[8] M. Forest, W.J.R. Hoefer, "Progrès dans la synthèse de structure électromagnetique par inversion du temps", Conference digest NUMELEC'92, Grenoble, France, March 1992.

[9] M. Forest, W.J.R. Hoefer, "TLM Synthesis of Electromagnetic Structures Using Time Reversal", Conference Digest, International Microwave Symposium, IEEE MTT-S, Albuquerque N.M., June 1992.

[10] M.A. Strickel, A. Taflove, " Time-Domain Synthesis for Broad-Band Absorptive Coating for Two-Dimensional Conducting Targets", *IEEE Trans. Antennas and Propagation*, Vol. AP-38, No. 7, July 1990.